THEORY OF ROD AND HALF ROD CONCENTRATED SOLAR CELLS

A Thesis

Presented To

THE FACULTY OF GRADUATE STUDIES

THE UNIVERSITY OF MANITOBA

In partial fulfillment

of the requirement for the degree of

MASTER OF SCIENCE

in

PHYSICS

by

IBRAHIM M. ABDEL-MOTALEB

July, 1982

THEORY OF ROD AND HALF ROD CONCENTRATED SOLAR CELLS

BY

IBRAHIM M. ABDEL-MOTALEB

A thesis submitted to the Faculty of Graduate Studies of the University of Manitoba in partial fulfillment of the requirements of the degree of

MASTER OF SCIENCE

ABSTRACT

The simple theory of solar cells operation is discussed using the help of the energy level diagram. The equations governing doping level and currents of a one dimension solar cell are presented plus the limitations of conventional cells and the possible means of overcoming these limitations.

The advantages of a rod cell and the experiments done by Johnson are explained. The continuity equations and the photo-generation rate are derived in cylindrical coordinates. These equations are solved numerically and the behaviour of the short circuit current, the open circuit voltage, the efficiency and the fill-factor w.r.t., the surface recombination velocities and the cells dimensions are studied theoretically.

ACKNOWLEDGEMENT

The author would like to thank Dr. Card and Dr. Kao for their Physical electronics course, and is deeply indebted to Professor F. Konopasek and Dr. J.S.C. McKee for their guidance and help.

Sincere gratitude is also extended to my mother-in-law and my father for their encouragement and support during my studies.

TABLE OF CONTENTS

LIST OF FIGURES

LIST OF SYMBOLS USED

a	Area of the cell
A_o	Junction perfection factor
AMO	Air mass O
AM1	Air mass 1
A.R	Antirefractive coating
B.S.F.	Back surface field
E	Electric field
G	Generation rate
F	Incident light intensity
F.F	Fill Factor
H	Thickness of a conventional cell
I_{dark}	Dark current
I_{ph}	Photo current
I_{sc}	Short circuit current
I_o	Saturation current
J_{ph}	Photo current density
J_{sc}	Short circuit current density
K	Boltzmann's constant
L_p, L_n	Holes and electron diffusion lengths
ℓ	Cell length
N_d	Donor concentration density
N_a	Acceptor concentration density
n_i	Intrinsic concentration density
n, p	Excess minority carrier concentration densities

n_p, P_n	Minority carrier concentration densities
n_{po}, p_{no}	Minority carrier concentration densities at equilibrium
q	Electron charge
R	Reflection coefficient
r_o	Cell radius
r_j	Junction radius
r_1	Length of the metallic contact from the cell center
R_s	Series resistance
R_{sh}	Shunt resistance
S	Surface recombination velocity on the top surface
S_1	Surface recombination velocity on the $\phi = 0$, $\phi = \phi_{max}$ surfaces
T	Temperature
W	Depletion region width
V_j	Junction voltage
V_d	Built in potential
$V_{o.c}$	Open circuit voltage
ε	The permetivity
ϕ_{max}	Maximum angle
τ_n, τ_p	Life times
α	Absorption coefficient
D_n, D_p	Diffisuion constant
σ_n, σ_p	Capture cross-sections
μ_p, μ_n	Holes and electrons mobilities
η	Efficiency
ρ	Resistivity

CHAPTER I.

INTRODUCTION

CHAPTER I

INTRODUCTION

A solar cell is a photovoltaic device designed to convert sunlight into electrical power and to deliver this power to a suitable load in an efficient manner. The advantage of solar cells lies in their ability to provide nearly permanent, uninterrupted power at no operating cost with only heat as a waste product, and their conversion of light directly into electricity rather than some intermediate form of energy. They also have a high power/weight ratio compared to other power sources. Their chief disadvantage lies in the low power/unit area, their relativity low efficiency, and high cost.[1]

The traditional silicon solar cell consists of a Si single crystal "wafer" 12-18 mils thick having a very thin (0.2-0.5) μm) diffused region at the surface to form a P-N junction. Electrical contact is made to the diffused region in such a way as to allow a maximum amount of light to fall on the Si element. An ohmic contact is to the back of the wafer. An evaporated antireflection coating is made applied to reduce the amount of light lost by reflection from the surface. Finally a cover of glass quartz, sapphire, or specially treated glass, with additional antireflection and ultraviolet rejection filters, is bonded to the cell with transparent adhesive to prevent high energy particles from reaching and degrading the device. The optimum material in terms of efficiency is a semiconductor with band-gap around 1.5 eV. Materials with band gaps from 1.1 to 2.0 eV are

nearly as good. The chief candidates are Si, InP, GaAs, CdS. Of all the available semiconductor, Si is the most abundant, the least expensive and whose technology is the most advanced.

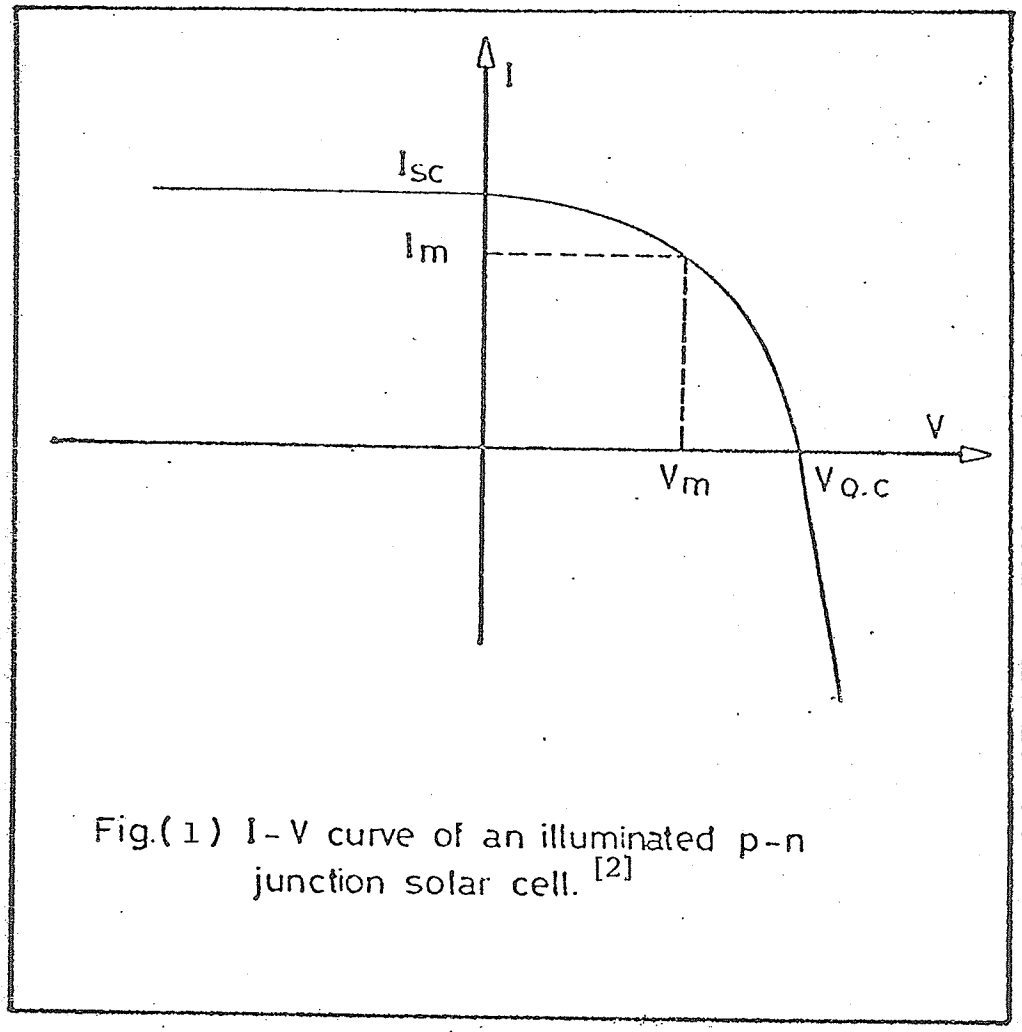

Fig.(1) I-V curve of an illuminated p-n junction solar cell. [2]

1.1 Device Parameters

Solar cell behavior can conveniently be examined through three main parameters (as shown in Fig. 1).

(a) The Open Circuit Voltage V_{oc}

this is the voltage output when the load impedance is much greater than the device impedance.

(b) The Short Circuit Current I_{sc}

this is the current output when the load impedance is much smaller than the device impedance.

(c) The Fill Factor F·F

this is the ratio of maximum power output to the product of V_{oc} and I_{sc}.

The efficiency of the cell can be expressed in terms of the above parameters by the relation

$$\eta = \frac{F \cdot F \; I_{sc} \cdot V_{oc}}{P_{in} \cdot a}$$

where a is the surface area of the device.

1.2 Literature Survey

The effort in Si can be divided into two main parts: a low cost material effort and a device improvement effort.[3]

Two paths of device improvement are underway: (1) to obtain higher efficiency cells (possibly at higher cost) and (2) to produce less expensive cells (probably at lower efficiency). High efficiency cell development received a boost several years ago with the advent of the "violet cell" which used narrow junction depth and reduced surface state concentrations to eliminate the dead layer at the surface of the diffused region, enhancing the photocurrent. The photocurrent had been enhanced by texturing the surface[2],[3] as shown in Fig. 2 and by using improved anti-reflection coatings of Ta_2O_5 together with silica cover glasses. The reflection loss has been reduced to 3% in this way and photocurrents of 46 mA/cm^2 (AMO) have been obtained.

Attempts are underway to reduce the cost of Si cells in four possible ways: by lowering the processing costs of conventionally designed cells, by automating the processing, by using hetrojunctions, and by using Schottky barriers. Lower cost processing techniques include screen printing of the contacts, spin-on anti-reflection coatings, and painted-on diffusion surfaces.[3] A sodium hydroxide etch is used to remove the damaged area from the Si surface after crystal sawing and to texture the surface as in Fig. 2. All these techniques have

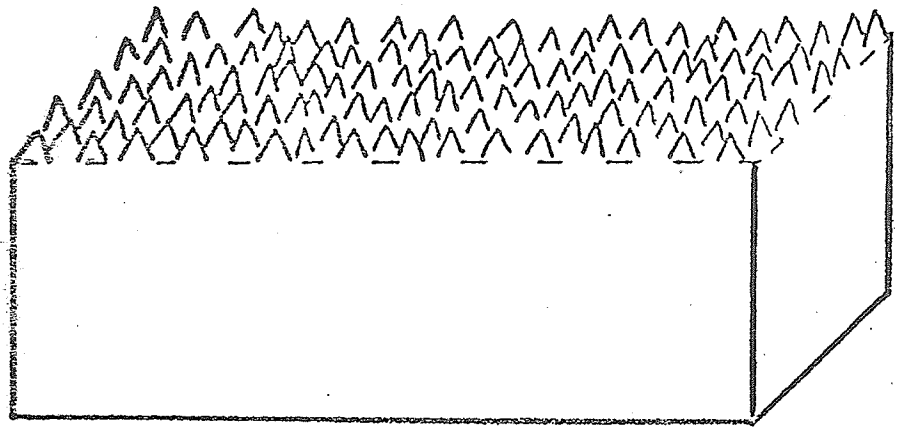

Fig.2 Textured surface of a high efficiency Si cell. [3]

proven successful and have produced 10-13% efficient cells (AMO).

A radically different structure that could lead to lower cost Si cells is the heterojunction cell shown in Fig. 3. A wide band gap material such as SnO_2, In_2O_3, Cds, or GaP is deposited upon an n-type or p-type Si substrate. The wide band gap material acts as a "window" passing most of the light into the silicon. Short wavelength light is absorbed within the depletion region in the Si, enhancing the blue response of the cell, while the long wavelength response is good if the diffusion length in the Si is high. Materials such as SnO_2 and In_2O_3 are inexpensive and easy to apply, leading to a potential cost reduction. Good experimental results have been obtained on several different structures using these transparent, highly conducting glasses. Efficiencies of 12% at AM1 have been reported for SnO_2-NSi cells

Schottky barrier devices (Fig. 4) are another potentially low cost method for obtaining terrestrial Si cells. A very thin metal film (75-150 A°) of Au, Ag, Cr, Cu, Aℓ, and the like are applied to a Si substrate, usually by evaporation. The metal film is thin enough to transmit most of the light into the Si. A thin oxide, 10-20 A° thick, is intentionally incorporated between the metal and the Si; it has been found that such an interfacial oxide enhances the voltage output (by lowering the dark current) without affecting the photocurrent.[3]

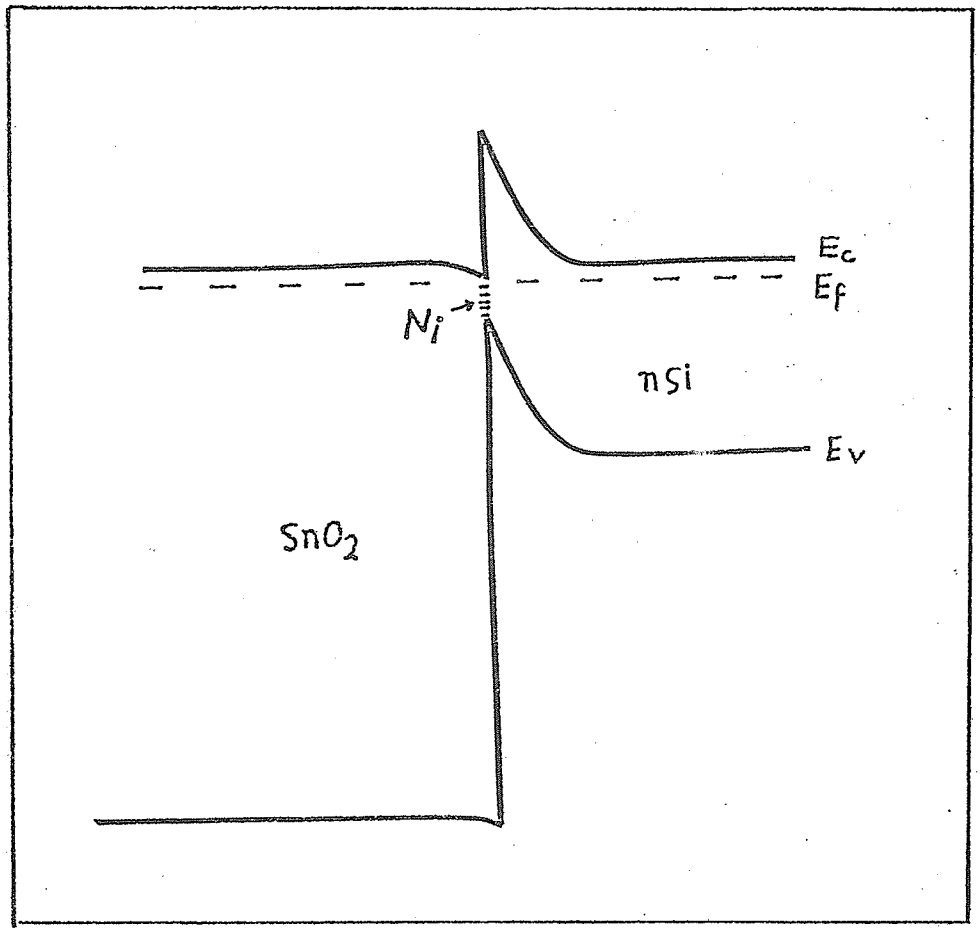

Fig. 3 Energy band diagram of a S_i-SnO_2 heterojunction solar cell.

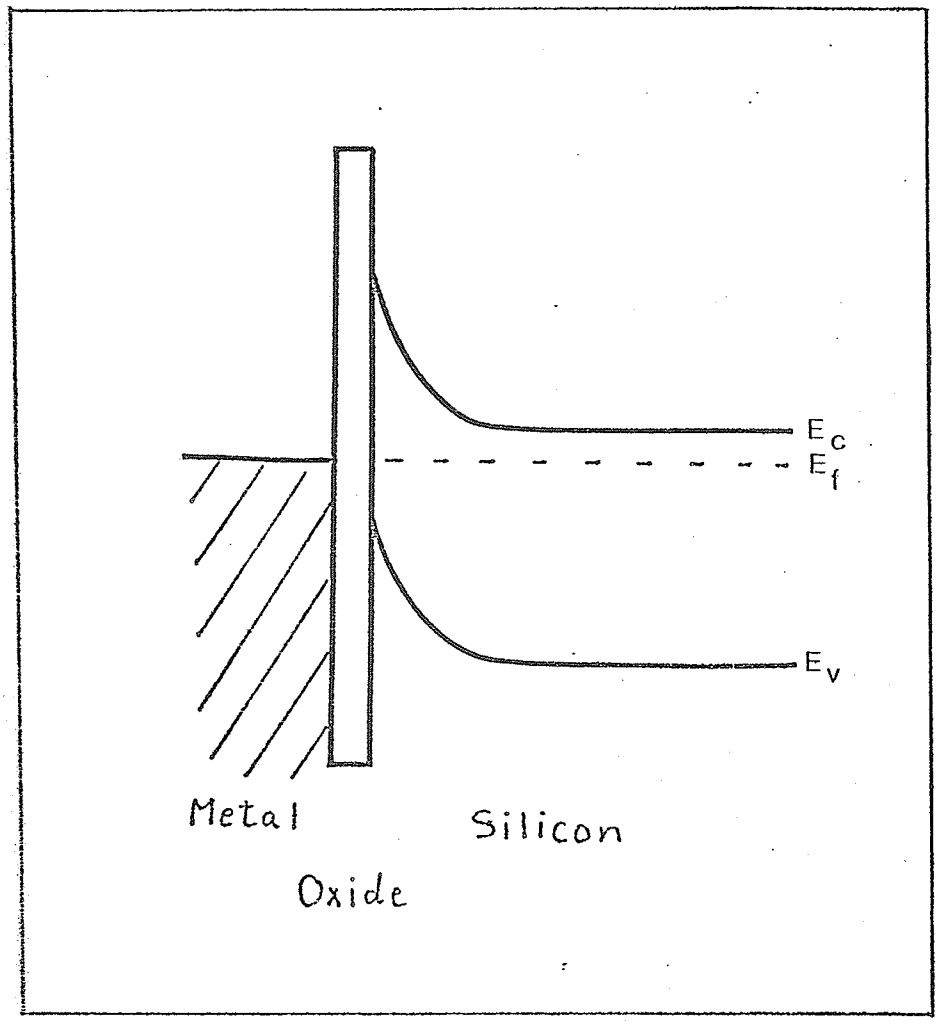

Fig. 4 Energy band diagram of a metal-oxide-S_i Schottky barrier solar cell.

1.3 The Thesis Objective

The objective of this thesis is to study theoretically a Rod and Half Rod silicon cell and the optimum dimensions for this cell. Such cells will be used in trough nontracking concentrator system.

CHAPTER II.

QUANTITATIVE ANALYSIS OF ONE-DIMENSIONAL SOLAR CELLS

CHAPTER II

QUANTITATIVE ANALYSIS OF ONE DIMENSIONAL SOLAR CELLS

2.1 Simple Theory of Single Crystal p-N Junction Solar Cells

If the junction is illuminated (Fig. 11) the incident photons are absorbed at different depths depending on their energy compared to the width of the energy gap (Eg) of the semiconductor. These photons librate electron hole pairs. If these minority carriers (electrons on the P-type and holes on N-type) succeed in diffusing to the edge of the depletion region before they recombine they will be swept through the barrier. If the external circuit is shorted a current will flow, which is the photo-current (assuming negligible series resistance). If a load is connected, there will be a voltage drop, this voltage will be applied to the P-N junction in a forward sense causing a dark current in opposite direction of the photocurrent. The net current will be the superposition of two currents, (the photo-current and the dark current) as shown in Fig. 5. This can be explained with aid of the energy level diagrams of the junction as below.[2]

The flow of carriers in the p-N junction occurs by two mechanisms. Minority carriers are swept by the junction field down the barrier and that mechanism leads to the reverse saturation current while the majority carriers diffuse against the barrier.

Under open-circuit condition (Fig. 6-a) the external current is zero which means that the rate of flow of minority carriers in one direction is just counter-balanced by the rate of flow of majority carriers

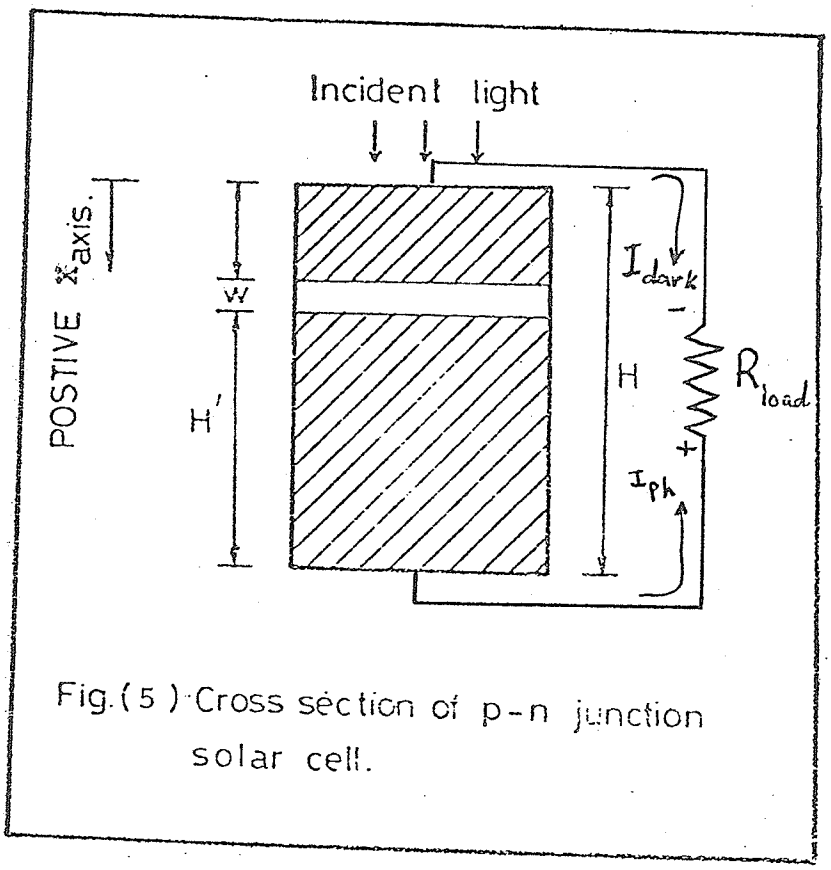

Fig.(5) Cross section of p-n junction solar cell.

of the same type in the opposite direction. If a reverse bias voltage is applied to the junction (Fig. 6-b) the barrier height increases. This increase in the barrier height does not affect the movement of minority carriers (the reverse saturation current), while it inhibits the diffusion of the majority carriers. If a forward bias voltage is applied to the junction (Fig. 6-c) the barrier height decreases. This again does not affect the drift of minority carriers. The diffusion of the majority carriers up the barrier is enhanced for a lower barrier in an exponential manner resulting in a large forward external current. The I-V curve for a simple P-N junction diode is shown in Fig. 7.

In an actual junction, current flow also results from recombination or generation (for forward bias and reverse bias respectively) within the depletion region. The total current for a practical junction can be written as

$$I = I_{oo} \left[\exp\left(\frac{qV}{A_o KT}\right) - 1\right] \qquad (1)$$

where

A_o - is called the diode ideality factor

A_o - is equal unity for a perfect junction and if A_o increases the density of traps inside the depletion layer increases.

The value of I_{oo} also depends on the traps in the depletion region, it increases with the trap density. For trap free junction I_{oo} is equal

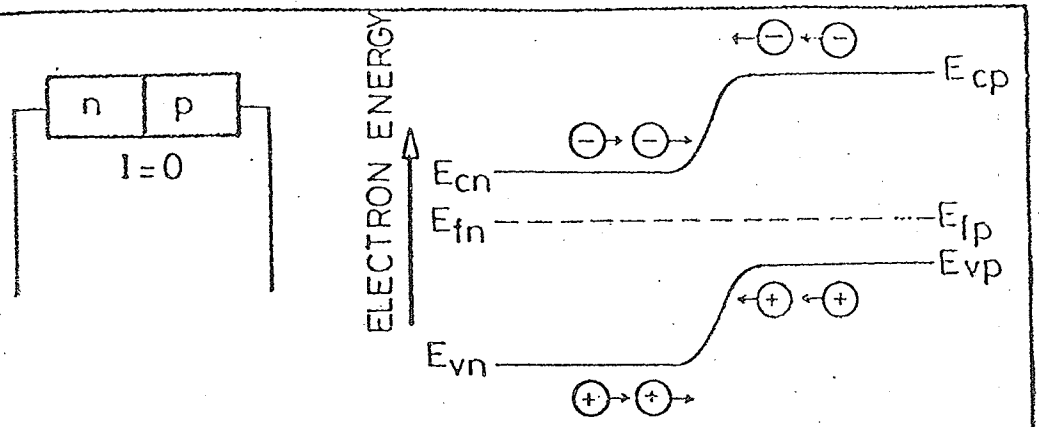

Fig. (6-a) p-n junction under open circuit condition.

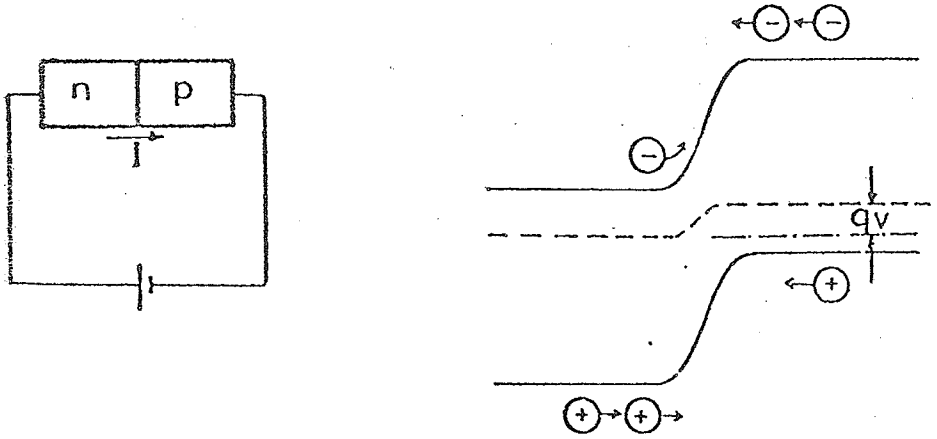

Fig. (6-b) p-n junction under reverse bias condition.

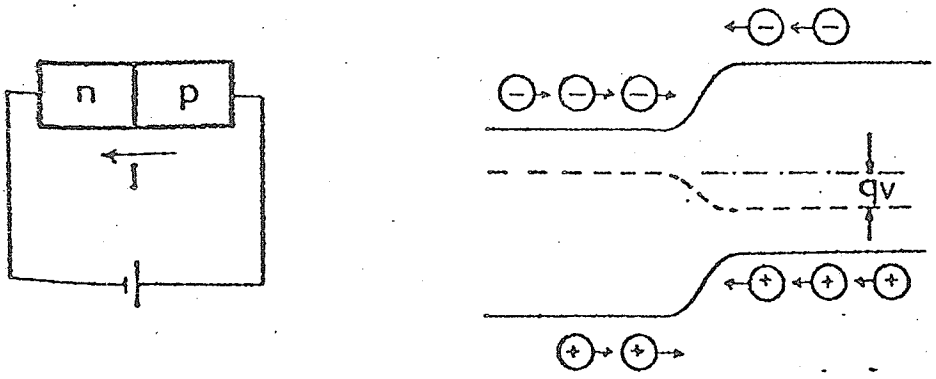

Fig.(6-c) p-n junction under forward bias condition. [2]

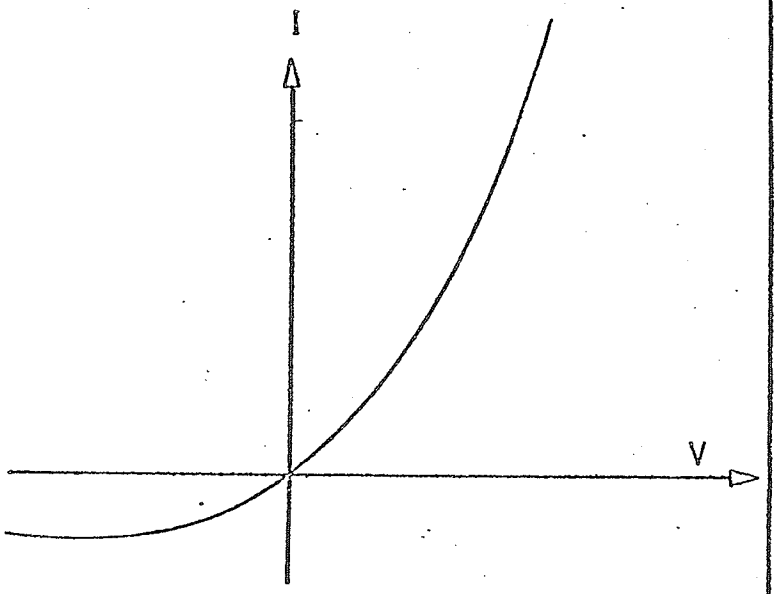

Fig. (7) I -V curve for a p-n junction diode in dark.

to the reverse saturation current (I_o) of a perfect junction.

The external junction current is the superposition of the photo-current (which is almost voltage independent) and the diode current. If the junction is reverse biased, the diffusion current is inhibitted and the external current is equal to the photo-current in addition to a very small reverse saturation current (Fig. 8-a). If the junction is forward biased the diffusion is enhanced since this current flows in a direction opposite to the direction of the photo-current, the external current then decreases (Fig. 8-b).

If the forward bias is gradually increased, the external current will decrease until the voltage reaches a value at which the dark current is equal and opposite to the photo-current, i.e. zero external current. This value of the junction voltage is the open circuit voltage V_{oc}.

If the junction voltage increases beyond V_{oc} the diffusion current dominates and the junction functions as a forward biased diode whose I-V curve is shifted along the current axis by I_{sc}

2.2 The Equivalent Circuit

Under normal conditions the solar cell feeds a passive load leading to a forward bias condition. Such a cell can be represented by the simple equivalent circuit shown in Fig. 9. The photo-current is represented by a current source I_{ph} and is opposite in direction to the forward bias current of the diode. Shunt resistance paths are represented by R_{sh} and series resistance represented by R_s

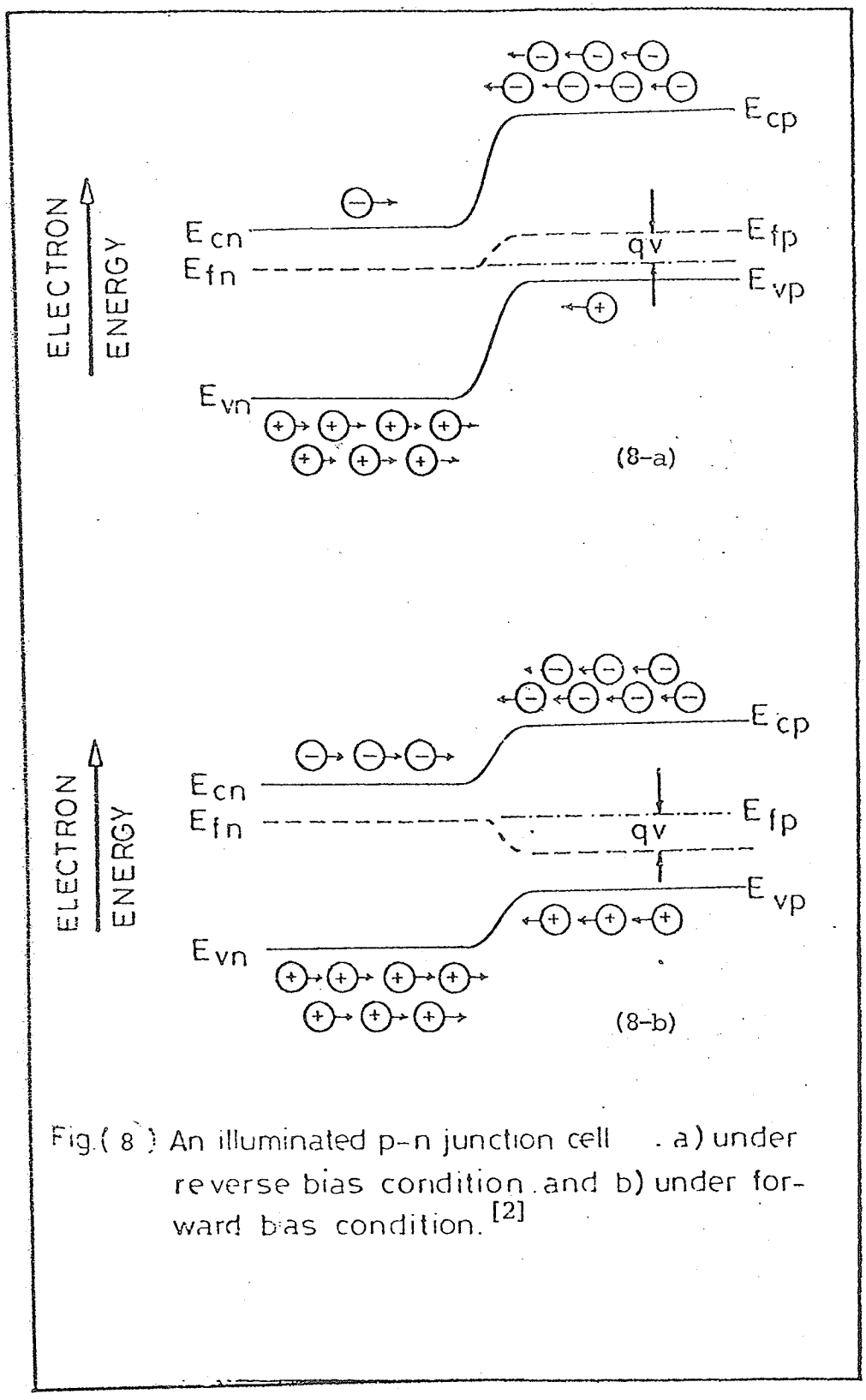

Fig.(8) An illuminated p-n junction cell . a) under reverse bias condition and b) under forward bias condition. [2]

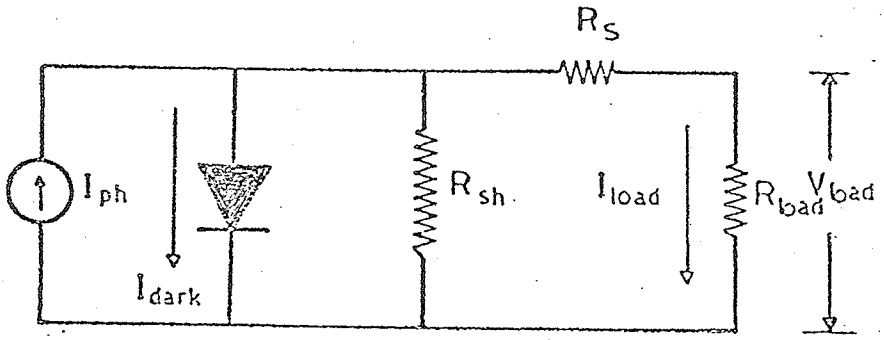

Fig.(9) Equivalent circuit of a solar cell under illumination. [1, 2]

2.3 Derivation of the Photo-current

When light of wavelength λ is incident on the surface of a semiconductor, the generation rate of electron-hole pairs as a function of distance x from the surface (Fig. 5) is

$$G(\lambda) = \alpha(\lambda)\ F(\lambda)(1 - R(\lambda))\exp\ (-\alpha(\lambda)x) \qquad (2)$$

where $F(\lambda)$ is the number of incident photons per cm^2 per sec per unit bandwidth. $R(\lambda)$ is the reflection coefficient. $\alpha(\lambda)$ is the absorption coefficient.

The photo-current that these carriers produce can be determined for low injection level condition using the minority carrier continuity equation[1]

For N-Region, continuity equation is:

$$\frac{1}{q}\ \frac{dJ_p}{dx}\ - G_p + (P_n - P_{no})/\tau_p = 0 \qquad (3)$$

The hole's current will be

$$J_p = q\ \mu_p\ P_n\ E - q\ D_p(dP_n/dx) \qquad (4)$$

when G_p is the Generation rate (2) for holes, E is the electric field, P_n is the photo-generated minority carrier density, P_{no} is the minority carrier density in the dark in equilibrium.

Since the continuity equation is linear, the general solution

is a superposition of the solutions over all wavelengths.

The boundary conditions applicable are:

$$D_p(d(P_n)/dx) - \mu_p P_n E = S_p(P_n - P_{no}) \quad \text{at } x = 0 \tag{5}$$

$$(P_n - P_{no}) = 0 \quad \text{at } x = x_j \tag{6}$$

where S_p is the surface recombination velocity due to the surface states on the surface at the top.

For the P Region, the continuity equation is

$$\frac{1}{q}\frac{dJ_n}{dx} + G_n - (n_p - n_{po})/\tau_n = 0 \tag{7}$$

The electron current is

$$J_n = q\,\mu_n\, n_p\, E + q\, D_n(dn_p/dx) \tag{8}$$

where G_n is the Generation rate for electrons, n_p is the photo-generated minority carrier density and, n_{po} is the minority carrier density in equilibrium in the dark.

The boundary conditions applicable are:

$$n_p - n_{p_o} = 0 \quad \text{at } x = x_j + W \tag{9}$$

$$D_n \frac{dn_p}{dx} + \mu_n n_p E = - s_n(n_p - n_{p_o}) \tag{10}$$

where S_n is the surface recombination velocity at the back and W is the depletion region width.

If the doping is constant, the electric field E will be zero in equations (4), (5), (8), and (10).

For ohmic contact at the back of the cell this lead to $S_n = \infty$ in equation (10), so the equation will be

$$(n_p - n_{po}) = 0 \tag{11}$$

The solution of equation (3) with the boundary conditions (5), (6) for constant doping is

$$(P_n - P_{n_o}) = [\alpha F(1-R)\tau_p/(\alpha^2 L_p^2 - 1)]$$

$$\times \left[\frac{(s_p L_p/D_p + \alpha L_p) \sinh \frac{x_j - x}{L_p} + \exp(-\alpha x_j)\left(\frac{s_p L_p}{D_p} \sinh \frac{x}{L_p} + \cosh \frac{x}{L_p}\right)}{(s_p L_p/D_p) \sinh \frac{x_j}{L_p} + \cosh \frac{x_j}{L_p}}\right.$$

$$\left. - \exp^{-\alpha x}\right] \tag{12}$$

and the resulting hole photocurrent density per unit band width at the junction edge is

$$J_p = \frac{q F(1-R) L_p}{[\alpha^2 L_p^2 - 1]} \times$$

$$\left[\frac{(s_p L_p/D_p + \alpha L_p) - \exp(-\alpha x_j)((s_p L_p/D_p)\cosh x_j/L_p + \sinh x_j/L_p)}{(s_p L_p/D_p) \sinh(x_j/L_p) + \cosh(x_j/L_p)}\right. \tag{13}$$

$$\left. - \alpha L_p \exp(-\alpha x_j)\right]$$

The solution of equation (7) with the boundary conditions (9), (10) for uniform doping is

$$(n_p - n_{p_o}) = \frac{F(1-R)\tau_n}{(\alpha^2 L_n^2 - 1)} \exp[-\alpha (x_j + W)]$$

$$\left[\cosh \frac{x-x_j-W}{L_n} - \exp[-\alpha (x - x_j - W)]\right.$$

$$\left. - \frac{(S_n L_n/D_n)[\cosh H'/L_n - \exp(-\alpha H')] + \sinh H'/L_n + \alpha L_n e^{-\alpha H'}}{(S_n L_n/D_n) \sinh(H'/L_n + \cosh(H'/L_n)} \right.$$

$$\left. \sinh \left(\frac{x-x_j-w}{L_n} \right) \right] \qquad (14)$$

and the resulting electron photocurrent density per unit band width at the junction edge is

$$J_n = \frac{q\, F(1 - R)\alpha L_n}{(\alpha^2 L^2 - 1)} \exp[-\alpha (x_j + W)]$$

$$\cdot \left[L_n - \frac{((S_n L_n)/D_n)(\cosh H'/L_n - e^{-\alpha H'}) + \sinh H'/L_n + \alpha L_n e^{-\alpha H'}}{(S_n L_n/D_n)\sinh H'/L_n + \cosh H'/L_n} \right. \qquad (15)$$

where H' is the total cell thickness minus the junction depth and depletion width $H' = H - (x_j + W)$.

The Depletion Region

Some photocurrent collection takes place from the depletion region. The electric field in this region can be considered high enough that photogenerated carriers are accelerated out of the depletion region before they can recombine, so that the photocurrent per unit bandwidth is equal simply to the number of photons absorbed. The depletion region current is

$$J_{dr} = q\,F(1 - R)\,\exp(-\alpha\, x_j)\,[1 - e^{-\alpha W}] \qquad (16)$$

The total short circuit photocurrent at a given wavelength is

$$\vec{J}_{photo} = \vec{J}_n + \vec{J}_p + \vec{J}_{dr} \qquad (17)$$

All of the above equations can be transformed from their present form for N-P cells equivalent to P-N cells by interchanging L_n, D_n, τ_n, and S_n with L_p, D_p, τ_p and S_p, respectively.

2.4 Derivation of the Dark Current

In all P-N junctions, several current transport mechanisms can be present at the same time and the magnitude of each one is determined by the doping levels on the two sides of the junction and by the presence of any added energy barriers as in heterojunctions. These transport mechanisms with forward bias are:[1]

1. Injection of carriers over the junction barrier.

2. Recombination of electrons and holes within the depletion region.

3. The injection of carriers up to a portion of the barrier followed by tunneling into energy state within the band gap.

In the normal Si P-N junction device with 1 or 10 Ω-cm base material, the tunnelling current is not likely to be of importance compared to the other two, but in Si devices made with 0.01 Ω-cm bases, the tunnelling component will probably dominate.

1. Injected Current

The N-Region

The behavior of minority carriers is governed by the continuity equation, (minority carriers injected from P-side to N-side). The continuity equation for minority carrier in the N-Region is

$$\frac{1}{q}\frac{dJ_p}{dx} + (P_n - P_{no})/\tau_p = 0 \qquad (18)$$

and the current equation is

$$J_p = q\,\mu_p\,P_n\,E - q\,D_p(dP_n/dx) \qquad (19)$$

The boundary conditions applicable are

$$P_n = P_{no}\ \exp\frac{qV_J}{KT}\ \text{at } x = x_j \qquad (20)$$

$$S_p(P_n - P_{no}) = D_p \frac{d}{dx}(P_n - P_{no}) - \mu_p P_n E \quad \text{at } x = 0 \tag{21}$$

where

V_j = the voltage across the junction.

The maximum value that the photovoltage can theoretically have is the "built-in" potential V_d which is related to the band gap by

$$V_d = E_g - [E_c - E_f) - (E_f - E_v)$$

$$= KT/q \ \ell n \left(\frac{N_a N_d}{n_i^2}\right) \tag{22}$$

where N_a, N_d and n_i is the acceptor, the donor and the intrinsic charge carrier densities.

The P-Region

The continuity equation is

$$\frac{1}{q} \frac{dJ_n}{dx} - (n_p - n_{po})/\tau_n = 0 \tag{23}$$

and the current equation is

$$J_n = q \mu_n n_p E + q D_n \frac{dn_p}{dx} \tag{24}$$

The boundary conditions are

$$n_p = n_{po} \exp(qV_J/KT) \quad \text{at } x = x_J + W \tag{25}$$

$$S_n(N_p - N_{po}) = -D_n \frac{d(N_p - N_{p_o})}{dx} - \mu_n n_p E \text{ at } x = H \tag{26}$$

If we have uniform doping the electric field E will be zero in equation (19),(21), (24), and (26), and the solution will be

$$P_n - P_{no} = A_1 \cosh\left(\frac{x}{L_p}\right) + B_1 \sinh\frac{x}{L_p} \qquad x \le x_J$$

$$n_p - n_{po} = A_2 \cosh[(x-(x_j + w))/L_n) \tag{27}$$

$$+ A_2 \sinh[(x-(x_j + w))/L_n] \quad x_j + w \le x \le H \tag{28}$$

and using the boundary conditions, the injected current becomes

$$J_{inj} = J_o(\exp[qV_j/KT] - 1) \tag{29}$$

where

$$J_o = q\frac{D_p}{L_p}\frac{n_i^2}{N_d}\left[\frac{(s_pL_p/D_p)\cosh(x_j/L_p) + \sinh(x_j/L_p)}{(s_pL_p/D_p)\sinh(x_j/L_p) + \cosh(x_j/L_p)}\right]$$

$$- q\frac{D_n}{L_n}\frac{n_i^2}{N_a}\left[\frac{(s_nL_n/D_n)\cosh(H'/L_n) + \sinh(H'/L_n)}{(s_nL_n/D_n)\sinh H'/L_n) + \cosh(H'/L_n)}\right] \tag{30}$$

2. Space Charge Layer Recombination Current

When a P-N junction is forward biased, electrons from the N-side and holes from the P-side are injected across the junction depletion region into the P- and N-side respectively, but at the same time some of these carriers recombine inside the depletion region, resulting in an increase in the dark current[5, 6]. This is the space charge layer recombination current. In the Sah-Noyce-Shockley (S-N-S) theory, the doping levels were assumed to be the same on the two sides of the junction and a single recombination center located in the vicinity of the center of the gap was assumed. This component

of the dark current was shown to be

$$J_{rg} = \frac{q\, n_i\, W}{\sqrt{\tau_{p_o}\, \tau_{n_o}}} \quad \frac{2 \sinh(q\, V_j/2KT}{q(V_d - V_j)/KT} \quad F(b) \tag{31}$$

where V_d is the built-in voltage, W is the depletion region thickness, and τ_{po}, τ_{no} are the minority carrier lifetimes on the two sides of the junction, and

$$F(b) = \int_0^\infty \frac{dx}{x^2 + 2bx + 1} \tag{32}$$

where

$$b = [\exp(-q\, V_j/2KT)]\, \cosh[(E_t - E_i)/KT + \tfrac{1}{2}\, \ell n(\frac{\tau_{p_o}}{\tau_{no}})], \tag{33}$$

where E_i is the intrinsic Fermi level.

3. Tunneling Current

Tunneling can be a major contribution to the dark current in 0.01 Ω-cm Si devices, heterojunctions such as Cu_2S-CdS, and for Schottky barriers. These tunneling currents take the form [7]

$$J_{tun} = K_1\, N_t\, \exp(B\, V_j) \tag{34}$$

where K_1 is a constant containing the effective mass, built-in barrier, doping level, dielectric constant, and Planck's constant, N_t is the density of energy states available for an electron or hole to tunnel

into, and

$$B = \left(\frac{4}{3h}\right) \left(m^* \varepsilon / N_{d,a}\right)^{\frac{1}{2}} \tag{35}$$

The only method for differentiating tunneling currents from thermal ones such as J_{inj} and J_{rg} is by temperature measurements. Tunneling is very insensitive to temperature while the opposite is true for thermal currents.

When more than one dark current component is present, the total dark current is the sum

$$\vec{J}_{dark} = \vec{J}_{inj} + \vec{J}_{rg} + \vec{J}_{tun}. \tag{36}$$

From the equivalent circuit (Fig. 9), the relation between the output current I_{out} and the output voltage V_{out} is

$$I_{out} \left(1 + R_s/R_{sh}\right) = I_{ph} - \left(V_{out}/R_{sh}\right) - I_{dark} \tag{37}$$

If $R_s \to 0$ $R_{sh} \to \infty$, equation (37) reduces to

$$I_{out} = I_{ph} - I_{dark}$$

The actual operating point on a given solar cell I-V characteristics (Fig. 1) is determined by the value of the load resistance R_L, and it is clearly desirable to choose R_L so that biasing occurs at the maximum power point (I_{max}, V_{max}). The energy conversion efficiency is then given by

$$\eta = \frac{I_{max}, V_{max}}{P_i \cdot a} \tag{38}$$

a is the surface area of the device.

The incident sunlight power density (P_i) at any position on earth depends on the thickness of the atmosphere between the observation point and the sun.

The air mass number (AM) is a measure of this thickness. AMO refers to the sunlight outside the atmosphere, while AM1 refers to the spectrum on earth when the sun is overhead. Figure 16 shows the spectral distribution for AM1 and AMO.

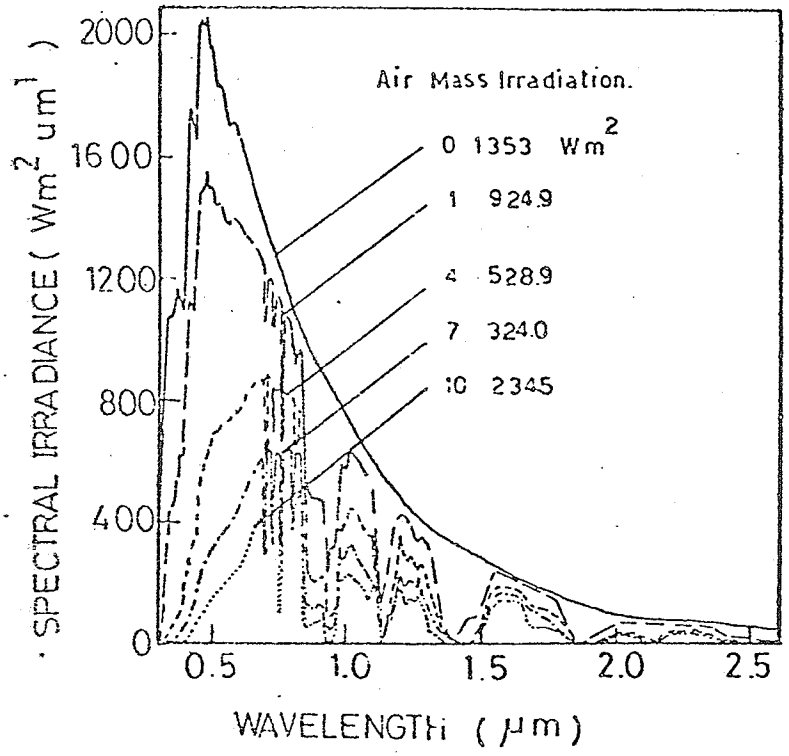

Fig.(10) Solar irradiance for different air mass values [2], [8]

CHAPTER III.

THE LIMITATIONS OF CONVENTIONAL SOLAR CELLS AND POSSIBLE MEANS OF OVERCOMING THESE LIMITATIONS

CHAPTER III

The Limitations of Conventional Solar Cells and the Possible Means for Overcoming these Limitations

3.1 The Band Gap

When the incident photons have energy greater than the band gap, absorption of the photons can take place and electrons can be raised in energy from the valence band to the conduction band creating hole-electron pairs. If the minority carriers are able to diffuse to the edge of the space charge region before they recombine, they are swept across the junction giving rise to photocurrent, photovoltage and power into the load. The necessary energy for the creation of electron-hole pairs is equal to the energy gap, the excess energy of the photons contributes to lattice vibrations, meaning that it is dissipated as heat. The photons with energy less than the energy gap pass through the cell. The role played by the energy gap in matching the properties of the semiconductor to the portion of sun energy utilized in the generation of electron-hole pairs is illustrated in Fig. 17[9]. Fig. 18 shows the variation of the maximum efficiency with energy gap and temperature[10].

3.2 The Absorption Coefficient

The ability of a material to absorb light of a given wavelength is measured quantitatively by the absorption coefficient in cm^{-1}.

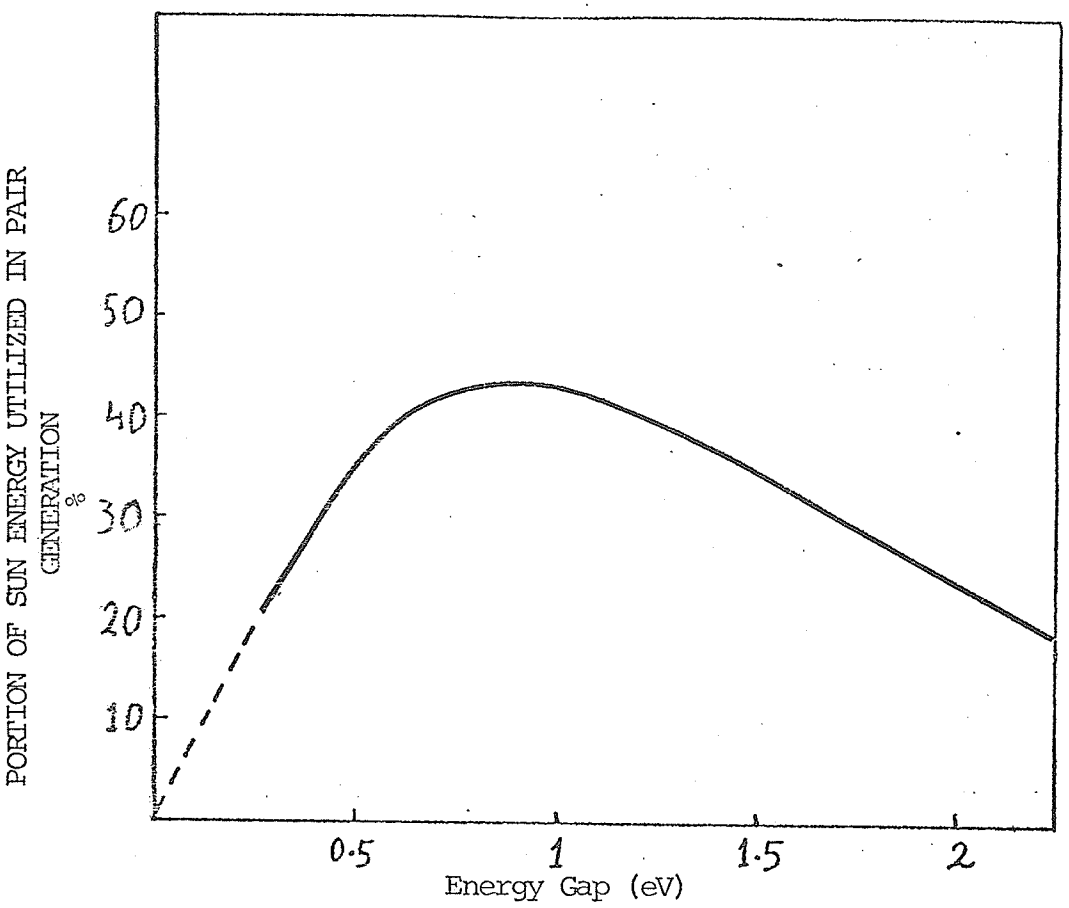

Fig. 11 The portion of the sun energy which can be utilized in electron-hole generation as a function of the width of the energy gap of the semiconductor. [9]

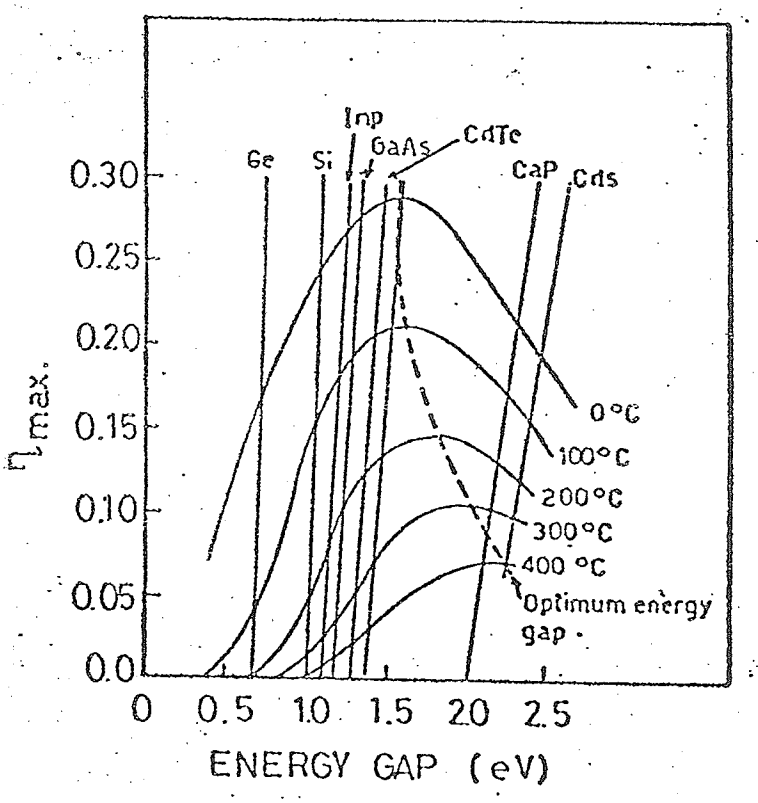

Fig.(12)Variation of the maximum efficiency with the energy gap and the temp. [10]

As a general rule the intensity falls exponentially. The absorption coefficient depends on the densities of states of the conduction band, the valence band, and on the directness or indirectness of the band gap and of the value of the band gap. Fig. 13 shows the intrinsic absorption coefficients for Si, Ge and Ga As.

3.3 The Reflection Coefficient

For Si the loss of the incident light due to the reflection amounts to 34% at long wavelengths (~1.1 μm) and rises to 54% at short wavelengths (~0.4 μm). To reduce the reflection coefficient, anti-reflective coatings can be used which reduce the reflection coefficient to 10% average for single layer and to 3% for double layer[1].

3.4 The Life Time

The collection of photogenerated carriers by motion across the P-N junction is in competition with the loss of these carriers by bulk and surface recombination before they can be collected. Bulk recombination can occur by band to band recombination, where an electron in the conduction band drops to the valence band to recombine with a hole and emits a photon, but annihilation through an intermediate recombination is usually the dominant mechanism. Fig. 14 shows the different recombination processes in the bulk of the semiconductor.

If there are N_r recombination centers of a single energy level E_r and having capture cross-sections σ_n and σ_p for an electron when empty, and hole when filled, respectively, then the hole life time

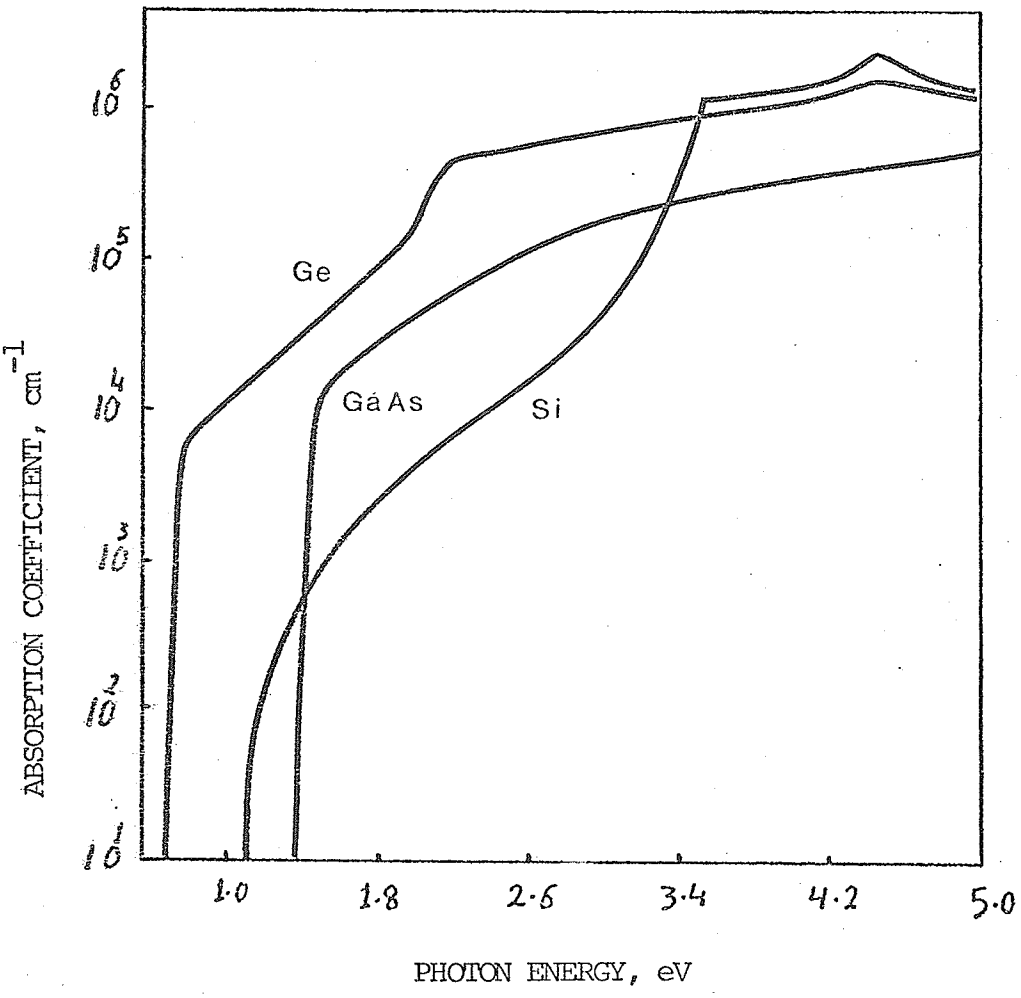

Fig. 13 Absorption coefficients of Si, Ge, GaAs [1]

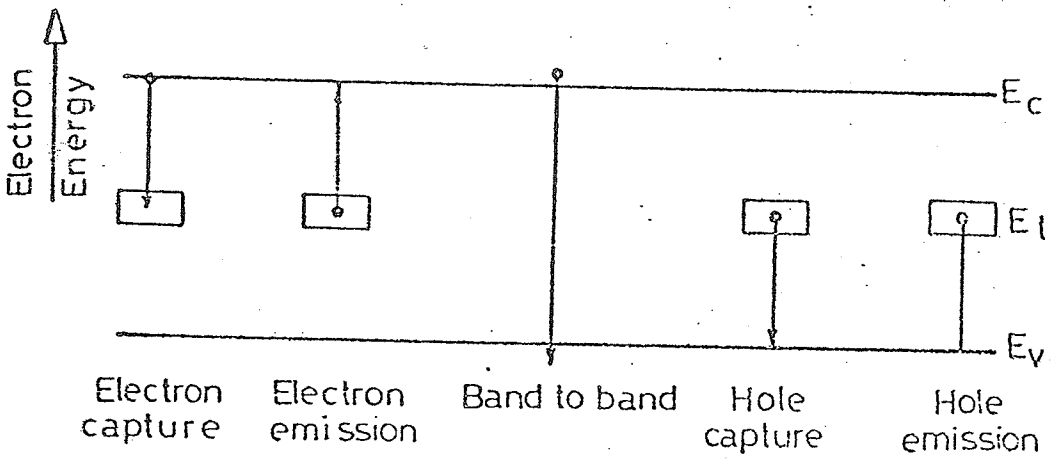

Fig. (14) Recombination process. [11, 12]

on the n-side of the junction is given by: [11]

$$\tau_p = \left(\frac{1}{\sigma_p V_{th} N_r} \right)\left[1+\left(\frac{N_c}{n_{no}}\right) \exp\left(1 - \frac{E_c - E_r}{KT}\right)\right.$$

$$\left. + \left(\frac{\sigma_p}{\sigma_n}\right) \left(\frac{N_v}{n_{no}}\right) \exp\left(- \frac{E_r - E_v)}{KT}\right)\right] \qquad (39)$$

where n_{no} is the free electron concentration on the n-type side and is essentially equal to the doping concentration, V_{th} is the thermal velocity, N_c and N_v are the densities of states in the conduction and valence band respectively, E_c and E_v are the conduction and the valence band edges respectively.

An analogous equation can be written for the electron lifetime in a p-type material.

Large values of lifetime result in high probability that carriers cross the depletion region leading to high current.

3.5 The Surface Recombination Velocity

In addition to recombination in the bulk, a loss of photogenerated minority carriers also takes place at the surface of the material due to the presence of surface states which arise from chemical residues, native oxides and the like. The rate at which carriers are lost at a surface is dependent on the surface recombination velocity S and the minority carrier density toward the surface and is given by

$$J_s = q\, s_p (P_n - P_{no}) \quad \text{for N-Region} \qquad (40)$$

$$J_s = q\, s_n (n_p - n_{po}) \text{ for p - Region} \tag{41}$$

The recombination velocity at the illuminated surface is of critical importance, since the number of carriers generated for a given wavelength is highest at this surface and decreases exponentially with distance into the cell.

Recombination velocity at the back of the cell is not as critical, but its importance increases as cells are made thinner, particularly for lightly doped base regions.

Surface recombination at the front is even more important for direct band gap materials than for indirect ones. This is because for direct gaps, a larger portion of carriers are generated close to the surface.

To reduce the effect of the surface recombination velocity one needs to provide (a) an electric field in one or both regions of the cell, (b) a back surface field.

Providing an electric field in one or both regions of the cell will aid in moving the photogenerated carriers toward the junction, where the energy band edges are sloping (rather than flat). The field at any point is given by

$$\begin{aligned} E &= 1/q\, dE_c/dx \\ &= 1/q\, dE_v/dx \\ &= D/\mu\ 1/N\ dN/dx \end{aligned} \tag{42}$$

where N is the ionization impurity concentration.

This electric field aids the collection of carriers generated at low photon energies. The photocurrent and the dark current for constant electric field is discussed by H. J. Hovel[1].

In back surface field devices the front part of the cell is made in the normal way, but the back of the cell instead of containing just a metalic contact to the moderately high resistivity base has a very heavily doped region adjacent to the contact as shown in Fig. 21.

The potential energy barrier ψ_p (Fig. 15) between the two base regions tends to "confine" the minority carriers in the more lightly doped region away from the ohmic contact at the back with its infinite surface recombination velocity.

If $W_p \tilde{=} L_n$ (L_n is the diffusion length) in region (1), then some of the electrons that would have been lost at the back surface cross the P-N junction boundary instead, enhancing the short circuit current and increasing V_{oc} due to the effect ψ_p and the decrease of the dark current (because of the isolation of carriers from the back contact). B.S.F. effects are discussed in detail by H. J. Hovel[1].

3.6 Diode Ideality

The total current for a practical junction is indicated by equation (1)

$$I = I_{oo}(\exp \frac{qV}{A_o KT} - 1)$$

A_o and I_{oo} increases as the density of traps inside the depletion region

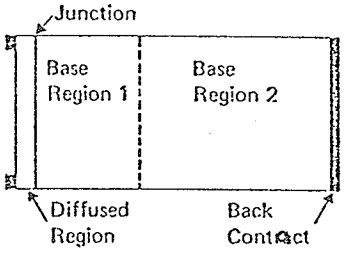

Fig. 15a Diagram of a solar cell in which the base can be divided into two regions with different doping levels, mobilities, lifetimes, and electric fields.

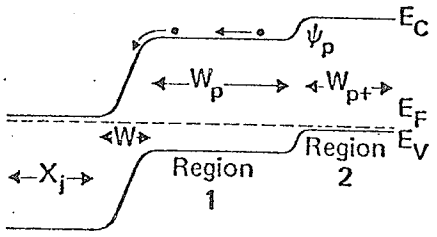

Fig. 15b Energy band diagram of a BSF device with a blocking back contact.

increases resulting in increasing the dark current. For a perfect junction $A_o = 1$ and 1_{oo} equals to the reverse saturation current.

3.7 The Series Resistance

The Fill factor is seriously reduced due to the series resistance because of the voltage drop across it leading to reduced output voltage and current. The short circuit current will be reduced below the value of the photo-current due to the forward bias across the diode caused by the voltage drop across R_s, which results in appreciable dark current as shown in Fig. 16a.

To reduce the effect of the series resistance, it is necessary to make the top region thin but very highly doped and to optimize the ohmic contact grid pattern, by increasing the number of fingers while decreasing the finger width and the distance between fingers. Fig. 16b shows the efficiency as a function of R_s.

3.8 The Shunt Resistance

Fig. 17a shows the effect of the shunt resistance on Si solar cell curves, where the fill factor and V_{oc} are reduced as the shunt resistance decreases. Fig. 17b shows the effect of R_{sh} on the efficiency where low R_{sh} leads to low efficiency. In general, surface passivation and careful preparation of the devices prevent significant shunt resistance problems.

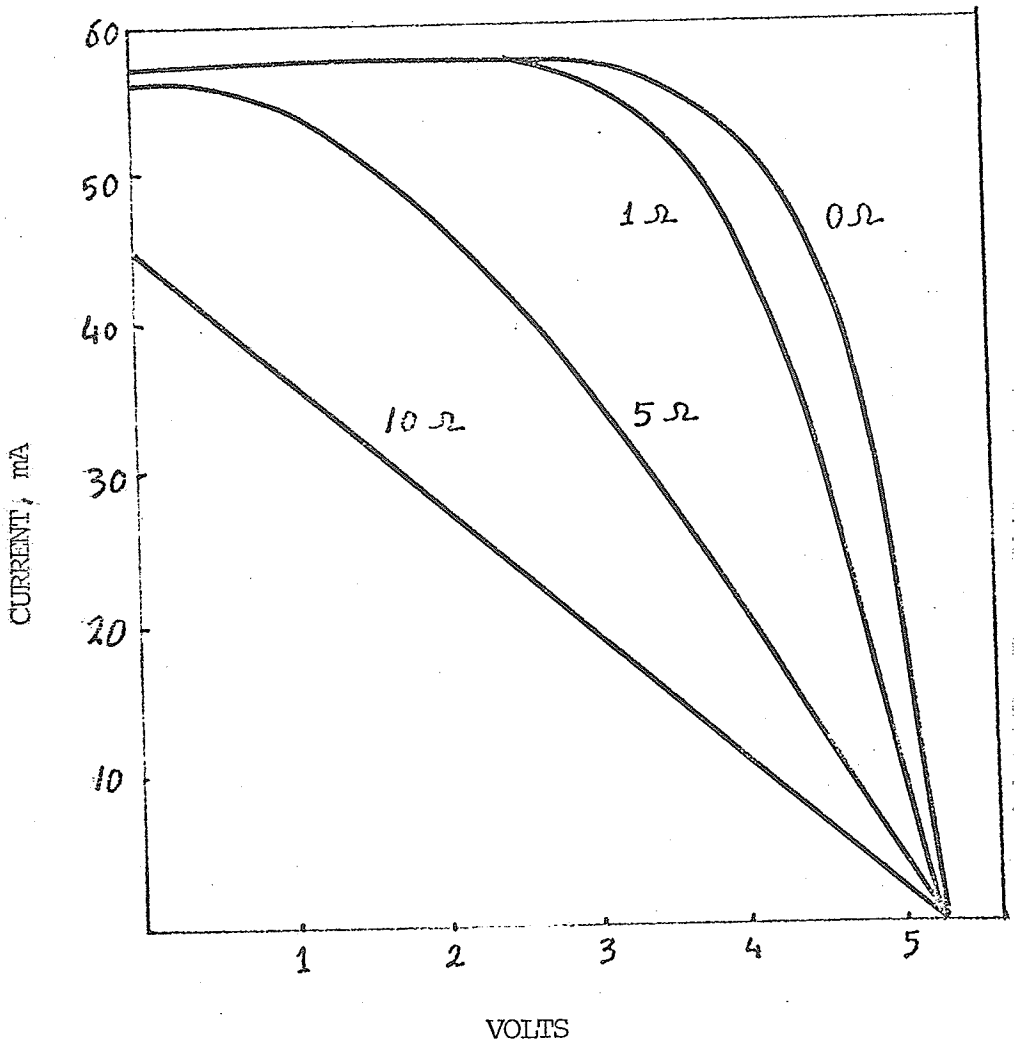

Fig. 16a The effects of series resistance on measured Si solar cell curves, Tungsten light, 100 mW/cm^2 cell area = 2 cm^2 [1].

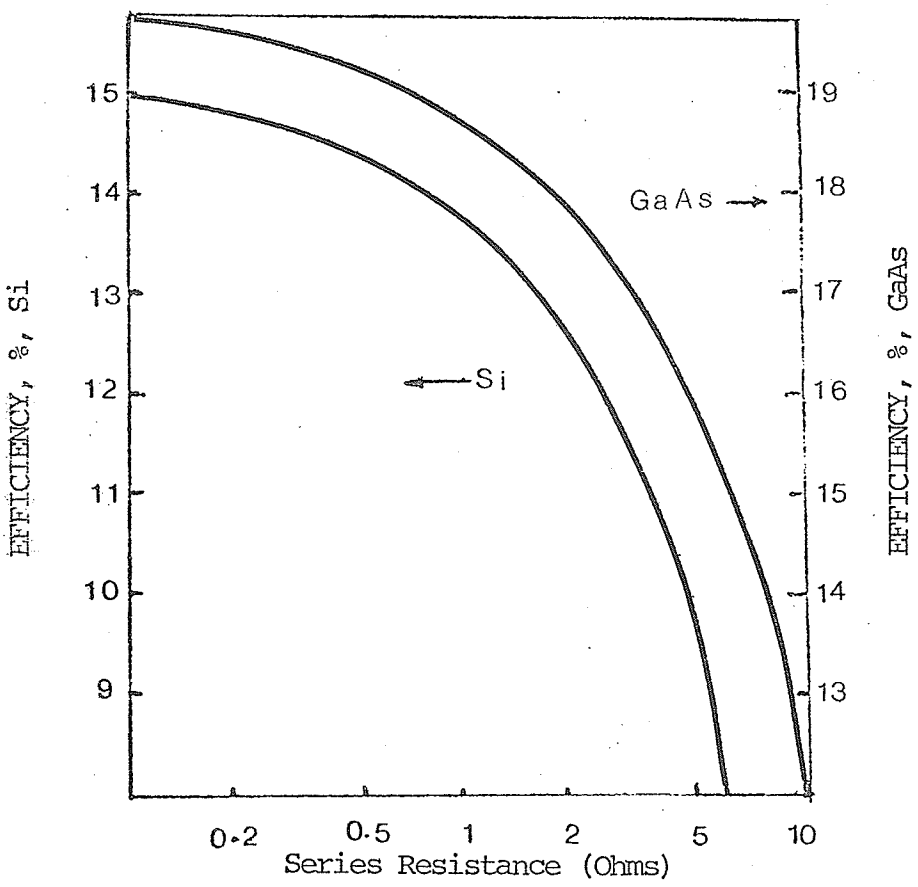

Fig. 16b The effects of series resistance on the AMO efficiencies of Si and GaAs solar cell [1].

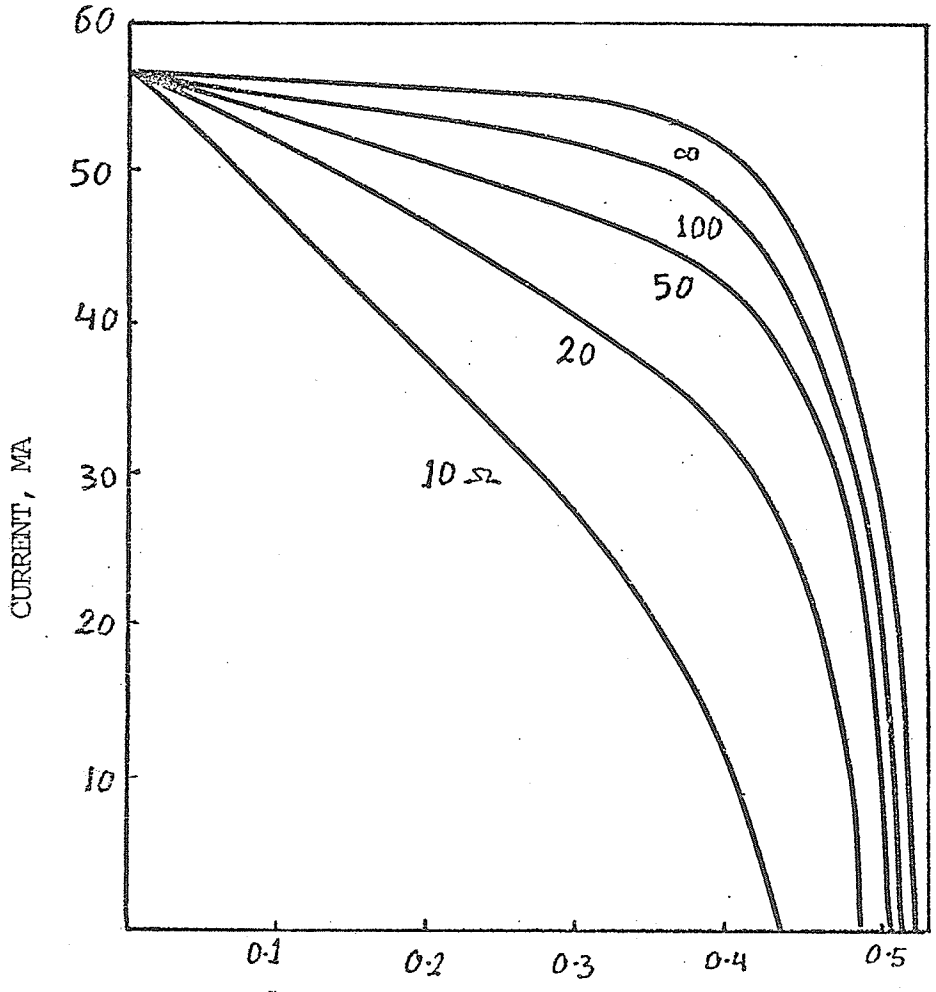

Fig. 17a The effects of shunt resistance on measured Si solar cell curves, same conditions as Fig. 16-a.

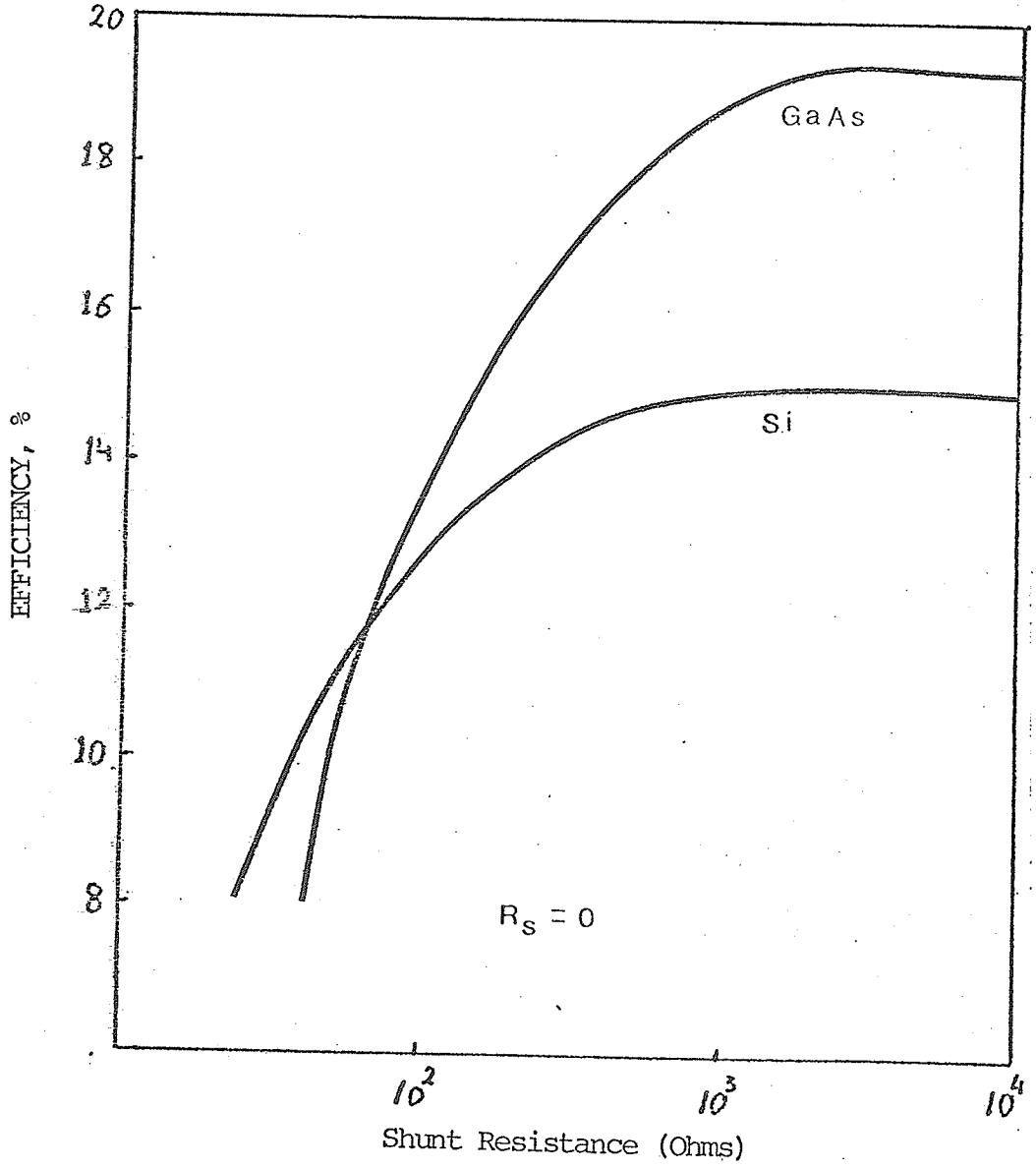

Fig. 17-b The effect of shunt resistance on the AMO efficiencies of Si and GaAs[1].

CHAPTER IV.

THEORETICAL ANALYSIS

CHAPTER IV

Theoretical Analysis

4.1 The Problem

One concept for reducing the cost of photo-voltaic arrays is the use of nontracking, trough-like sunlight concentrators especially the ideal shape for trough reflectors described by Winston[13] and Baranov[14]. This shape is said to be "ideal" because it achieves the maximum possible acceptance angle for a given degree of concentration. Fig. (18) shows the trough-like sunlight concentrators.

A major difficulty in using trough concentrators for photo-voltaic arrays has been the lack of a suitable shape of silicon cells. The basic problem is that linear concentrators require linear (i.e. elongated) energy receivers.

The obvious approach is to arrange conventional round wafer cells into a line at the bottom of the trough. This has two disadvantages :[15] (1) packing geometry prohibits receiving more than 78% of the concentrated sunlight, (2) for ordinary 75 mm wafers the reflections are necessarily very bulky.

Another approach has been the use of linear arrangements of diced, rectangular wafers[16]. Although this overcomes the previously mentioned problems, it introduces a new problem namely that of interconnecting large numbers of individual cells.

An ideal silicon geometry for use in trough concentrator would be a long, narrow ribbon such as that promised by the continuous

ribbon growth techniques. To date however this technique does not yield silicon from which high efficiency cells can reliably be made.

As an alternative to ribbon silicon cells, Johnson[15] has considered using solar cells on the surface of small diameter (4 mm) silicon rods.

This chapter presents a theoretical analysis of the cell fabricated by Johnson[15].

4.2 Rod Solar Cell - Experimental Results[15]

Johnson has developed a laboratory process to make two types of solar cells on 4 mm diameter silicon rod as shown in Fig. 19. The full rod design, which is intended for use in metallized reflectors, uses a copper fin to serve simultaneously as a mechanical support, an electrical contact, and as a heat dissipator. The half rod design is an adaptation for use in transparent dielectric concentrators which function by total internal reflections. G. Johnson reported that the solar cell performance is measured at several illumination levels using two quartz halogen bulbs, equidistant from and on opposite sides of the rod cell which are adjusted to each give a flux 157 mw/cm^2. He assumed that this is equivalent to 100 mw/cm^2 when averaged over the cylindrical surface. He reported that the best sample gave him nearly 14% efficiency over an area of ~ 7 cm^2 and I_{sc} = 33 ma/cm^2 (active area only), V_{oc} = 0.61 V, and FF = 0.77. Typical samples ranged from 10% - 13% in efficiency.

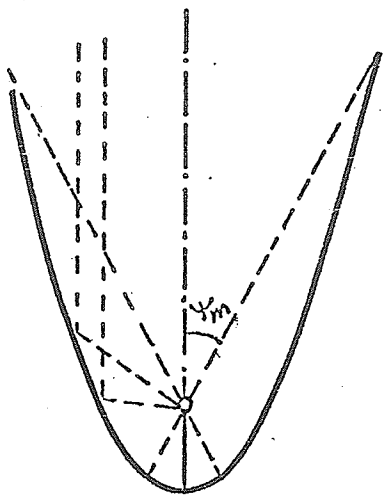

Fig. (18) Trough-like sunlight concentrator

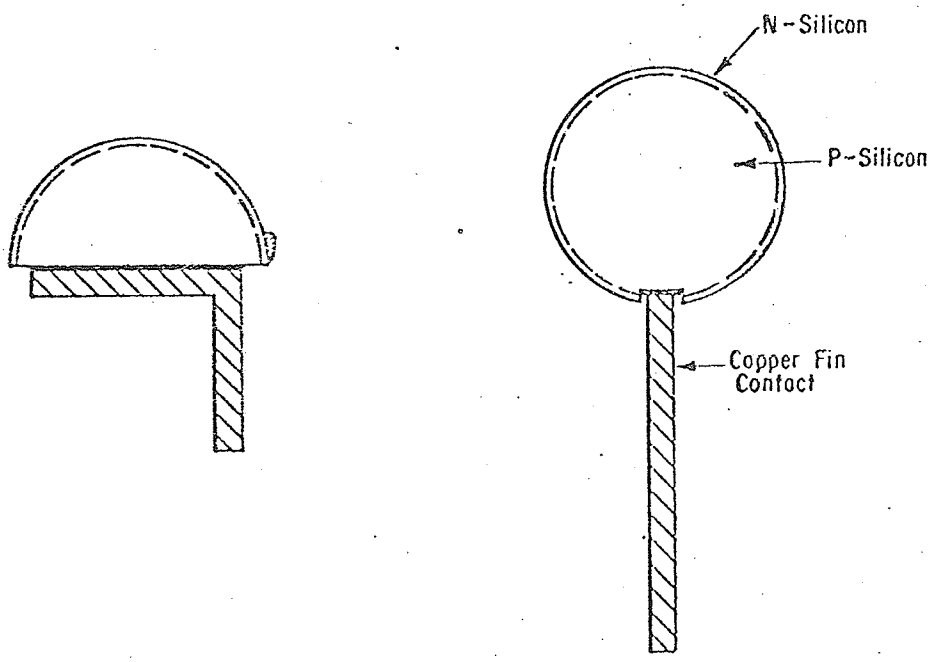

Fig. 19 Rod and Half-Rod Cells[15].

4.3 Model and Numerical Calculation for a Rod Solar Cell

In this work a model is introduced to study the characteristics of both full rod and half rod, where the full rod model is slightly different from the cell designed by Johnson, to facilitate theoretical calculations (Fig. 20). Assuming constant cell parameters and constant temperature at 300 K and constant intensity of incident sunlight over the surface of the cell, short circuit current and dark current are calculated.

4.3.1 Calculation of the Short Circuit Current

Under the assumption that the life time, mobility and the doping level are constant and no electric field exists outside the depletion region, the continuity equations is

$$\frac{\partial^2 P}{\partial r^2} + \frac{1}{r}\frac{\partial P}{\partial r} + \frac{1}{r^2}\frac{\partial^2 P}{\partial \phi^2} + \frac{G_p}{D_p} - \frac{P}{D_p \tau_p} = 0 \qquad (43)$$

for the n-type region, and

$$\frac{\partial^2 n}{\partial r^2} + \frac{1}{r}\frac{\partial n}{\partial r} + \frac{1}{r^2}\frac{\partial^2 n}{\partial \phi^2} + \frac{G_n}{D_n} - \frac{n}{\tau_n D_n} = 0 \qquad (44)$$

for the p-type region. The generation rate G_n and G_p in cylindrical coordinate is

$$G(\lambda) = \frac{r_o}{r} \cdot F(\lambda) \cdot (1 - R) \cdot (\alpha(\lambda) - \frac{1}{r}) \cdot e^{-\alpha(r_o - r)} \qquad (45)$$

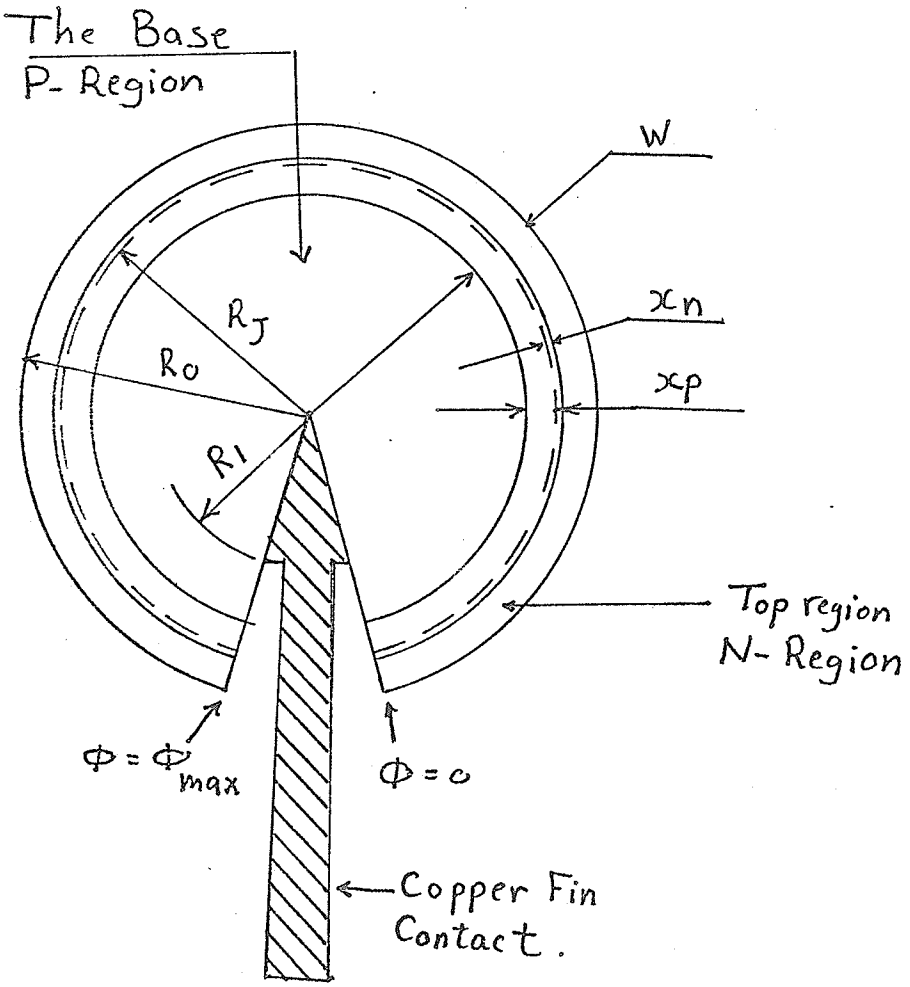

Fig. 20 Model of calculations.

It is assumed that the excess photogenerated minority carrier density reduces to zero at the back surface due to the ohmic contact and reduces to zero also at the edges of the depletion region due to the barrier electric field. The excess minority carrier densities at the top surface and at both $\phi = 0$ and $\phi = \phi_{max}$ edges are governed by the recombination velocities. So the boundary conditions can be written

$$D_p \frac{\partial P}{\partial r} = S_p P \qquad \text{at } r = r_o \tag{46a}$$

$$P = 0 \qquad \text{at } r = r_j + X_n \tag{46b}$$

$$D_p \frac{1}{r} \frac{\partial P}{\partial \phi} = p S_p \qquad \text{at } \phi = 0,\ r_o > r > r_j + X_n \tag{46c}$$

$$-D_p \frac{1}{r} \frac{\partial P}{\partial \phi} = P S_p \qquad \text{at } \phi = \phi_{max},\ r_o > r > r_j + X_n \tag{46d}$$

for n-region, and

$$n = 0 \qquad \text{at } r = r_j - X_p \tag{47a}$$

$$D_n \frac{1}{r} \frac{\partial n}{\partial \phi} = +S_n n \qquad \text{at } \phi = 0,\ r_j - X_p > r > r_1 \tag{47b}$$

$$-D_n \frac{1}{r} \frac{\partial n}{\partial \phi} = +S_n n \qquad \text{at } \phi = \phi_{max},\ r_j - X_p > r > r_1 \tag{47c}$$

$$n = 0 \qquad \text{at } \phi = 0,\ r < r_1 \tag{47d}$$

$$n = 0 \qquad \text{at } \phi = \phi_{max},\ r < r_1 \tag{47e}$$

for the p-region.

The continuity equations (43, 44, 45) were solved numerically using the boundary conditions mentioned before. Knowing the minority carrier distribution, we can obtain the short circuit current densities from the equations

$$J_p = - q D_p \frac{\partial P}{\partial r} \qquad \text{at } r = r_j + x_n \tag{48}$$

$$J_n = q D_n \frac{\partial n}{\partial r} \qquad \text{at } r = r_j - x_p \tag{49}$$

In addition to the currents densities given by (48), (49) the depletion region current is

$$I_{dr}(\lambda) = \phi r_o \, q \, F(\lambda)(1-R) \, e^{-\alpha(r_o - r_j - x_n)} \cdot [1 - e^{-\alpha w}] \cdot \ell \tag{50}$$

where

$$w = X_n + X_p = \sqrt{(2\epsilon_s/p) \frac{N_a + N_d}{N_a \cdot N_d} (V_d - V_j)}$$

4.3.2 Calculations of Dark Current

The continuity equations (43, 44) take the form

$$\frac{\partial^2 P}{\partial r^2} + \frac{1}{r} \frac{\partial P}{\partial r} + \frac{1}{r^2} \frac{\partial^2 P}{\partial \phi^2} - \frac{P}{D_p \tau_p} = 0 \tag{51}$$

for the n-type region, and

$$\frac{\partial^2 n}{\partial r^2} + \frac{1}{r} \frac{\partial n}{\partial r} + \frac{1}{r^2} \frac{\partial^2 n}{\partial \phi^2} - \frac{n}{D_n \tau_n} = 0 \tag{52}$$

for the p-type region.

Neglecting the effect of the series and shunt resistance, the junction voltage V_J will be equal to the terminal voltage and hence the density of the minority carriers at the edges of the depletion region are given by Boltzman's relationships (20), (25) and the density of the minority carrier reaches its thermal equilibrium value at the ohmic back contact. The density of the minority carriers at the top surface, at $\phi = 0$ and $\phi = \phi_{max}$ edges are governed by the recombination velocities there. The boundary conditions will be

$$D_p \frac{\partial P}{\partial r} = S_p P \qquad \text{at } r = r_o \tag{53a}$$

$$P_n - P_{no} = P_{no}(e^{+qV_J/KT} - 1) \qquad \text{at } r = r_j + X_n \tag{53b}$$

$$D_p \frac{1}{r} \frac{\partial P}{\partial \phi} = S_p P \qquad \text{at } \phi = 0,\ r_o > r > r_j + X_n \tag{53c}$$

$$-D_p \frac{1}{r} \frac{\partial P}{\partial \phi} = S_p P \qquad \text{at } \phi = \phi_{max},\ r_o > r > r_j + X_n \tag{53d}$$

for the n-region, and

$$n_p - n_{po} = n_{po}(e^{(qV_J/KT)} - 1) \qquad \text{at } r = r_j - X_p \tag{54a}$$

$$D_n \frac{1}{r} \frac{\partial n}{\partial \phi} = + S_n n \qquad \text{at } \phi = 0,\ r_j - X_p > r > r_1 \tag{54b}$$

$$-D_n \frac{1}{r} \frac{\partial n}{\partial \phi} = + S_n n \qquad \text{at } \phi = \phi_{max},\ r_j - X_p > r > r_1 \tag{54c}$$

$$n_p - n_{po} = 0 \qquad \text{at } \phi = 0,\ r < r_1 \tag{54d}$$

$$n_p - n_{po} = 0 \qquad \text{at } \phi = \phi_{max},\ r < r_1 \tag{54e}$$

for p-region.

The dark current densities is calculated from the equations (48), (49). The load current can then be calculated since

$$I_{load} = I_{ph} - I_{dark} \tag{55}$$

for different values of applied voltage. From the I-V curve, we obtain the value of the open circuit voltage and the maximum power point. The efficiency of the cell was calculated using the input solar power density for AMI of 100 mw/cm^2 and for AMO of 135 mw/cm^2.

The data used in the calculation is shown in table (1). High base resistivity δ_{base} gives a high life time cell of low bulk recombination, but at the same time the series resistance will increase and the problems mentioned in section 3.7 will appear.

The series resistance of a half rod can be written approximately as

$$R_s = \frac{\rho}{\pi \ell} \tag{56}$$

which is independent of the radius, so the decreasing of ρ_{base} is the only way to reduce R_s for a fixed length.

Low δ_{base} gives low series resistance cell but the bulk recombination will increase because of the decrease of the life time.

The chosed δ_{base} of 1 Ω-cm is suitable because it gives $R_s = 0.3$ for $\ell = 1$ cm and life time of 10×10^{-6} sec.

The numerical method used in calculation is Gaus-Seidel method[17], this method will be explained in appendix (c).

TABLE (1)

Top Region		Base Region	
N_d	5×10^{19} cm^{-3}	N_a	1.5×10^{16} cm^{-3}
D_p	1.295 cm^2/sec	D_n	27 cm^2/sec
τ_p	0.4×10^{-6} sec	ζ_n	10×10^{-6} sec

V_d	0.930 volt
n_i	1.6×10^{10} cm^{-3}
ε_s	11.8 ε
ρ_{base}	1 Ω-cm
E_g	1.12 eV
r_o	2 mm
r_j	1.9999 mm
T	300 K
R	3%

CHAPTER V.

RESULTS AND DISCUSSIONS

CHAPTER V

Results and Discussion

In this chapter the results of the calculations are presented and discussed.

5.1 Short Circuit Current: (I_{sc})

Figure 26 shows the short circuit current as a function of the surface recombination velocity on the top surface. It can be seen from the figure that as the surface recombination velocity S increases, the short circuit current decreases slightly for surface recombination velocity values less than 10^4 cm/sec and then decreases steeply for the values greater than 10^4 cm/sec. This is because the surface states on the top act as a sink for the minority carriers and as the rate of the surface recombination increases the minority carrier loss increases leading to the decrease of the short circuit current. The material used is silicon which has an indirect band gap, so most of the electron-hole pairs are generated far from the surface, so the effect of the surface recombination does not appear until the surface recombination velocities have high enough values. Figure 27 shows the short circuit current as a function of the surface recombination velocity S_1 at $\phi = 0$ and $\phi = \phi_{max}$ surfaces. As expected, increasing S_1 leads to decreasing short circuit current similar to the effect of the surface recombination velocity on the top surface. The effect of S_1 appears at values equal to 10^2 cm/sec, rather than 10^4 cm/sec in the case of S. This is because the great

part of the area of these surfaces is on the base region (Fig. 25) where most of the carriers generated there leads to great effect of small values of S_1 on I_{sc}. Increasing S_1 leads to the decrease of I_{sc} until it reaches a constant value.

Figure 28 shows that the increase of the top thickness causes a serious decrease in short circuit current. This decrease in short circuit is expected because the top region is very highly doped ($N_d = 5 \times 10^{19}$ cm^{-3}). This means it has a very low life time resulting in a high recombination rate inside the region, which results in a low short circuit current.

The variation of cell radius has great importance. This can be seen from Figure 29. In this graph one can see that if the radius increases the short circuit current also increases to a maximum, and then decreases to reach a constant value. This behavior can be interpreted by the aid of equation 45. The reason the short circuit current increases with radius is due two factors: (a) the loss of transmitted light decreases with increasing radius, (b) the influence of the back contact decreases (an ohmic contact of infinite surface recombination velocity). The reason for the existence of a maximum is the geometry of the cell. There are two terms in equation (45) which have opposite effects as r_o varies. First, the term $-1/r$ which reduces the Generation rate $G(\lambda)$, and second the term r_o/r which is greater than or equal to unity. If r_o is large, the term $-1/r$ tends to zero and the term r_o/r tends to unity while $G(\lambda)$ tends to the one dimensional case. This is the reason for the constant current values

for large radius. This interpretation appears correct because r changes from a maximum value to r_o to a minimum value below r_o by double the diffusion length within which distance nearly all the incident photons are absorbed. If r_o is few times the diffusion length, the effect of these two terms will appear, resulting in a maximum value of $G(\lambda)$ and thus a maximum value of I_{sc}. If r_o is smaller than the diffusion length the effect of the two factors (a) and (b) will be dominant and will govern the behavior of the cell.

5.2 The Open Circuit Voltage (V_{oc})

The value of the open circuit voltage as a function of the surface recombination velocities S_1, S and the thickness of the top region R_T is approximately constant at a value about 0.66 volt. Its value as a function of cell radius is not so constant. Figure 30 shows that if the radius increases, the open circuit voltage increases also, but to a limit and it then decreases to a constant value. This behavior is due to two influences: (i) the increase of the short circuit current due to the increase of the radius (factor (a) mentioned before), (ii) the increase of the dark current due to the increase of the amount of the bulk recombination if the radius increases.

The first effect tends to increase V_{oc} and the second tends to decrease V_{oc} leading to the behavior shown in Fig. 30.

5.3 Efficiency (η)

Figure 31 shows that as the surface recombination velocity S increases, the efficiency will decrease. This is simply because the increase of S leads to a decrease in I_{sc} meaning a decrease in the load current and consequently a decrease in efficiency. The effect of the increase of the surface recombination velocity S_1 is similar to that of S as shown in Fig. 32.

Figure 33 indicates the behavior of the efficiency as a function of the top thickness R_T. As R_T increases the efficiency decreases because of the decrease of I_{sc} due to the increase of R_T which leads consequently to a decreased load current.

Figure 34 shows the effect of the cell radius on the efficiency which is due to the behavior of I_{sc} and V_{oc} as a function of the radius as shown in Fig. 29 and Fig. 30.

5.4 The Fill Factor (F.F)

The Fill Factor does not change if S, S_1 and R_T changes. It has an approximate value of 83.9%. The Fill Factor as a function of the cell radius is shown in Fig. 35. The behavior depends on the behavior of the efficiency, the short circuit current and the open circuit voltage.

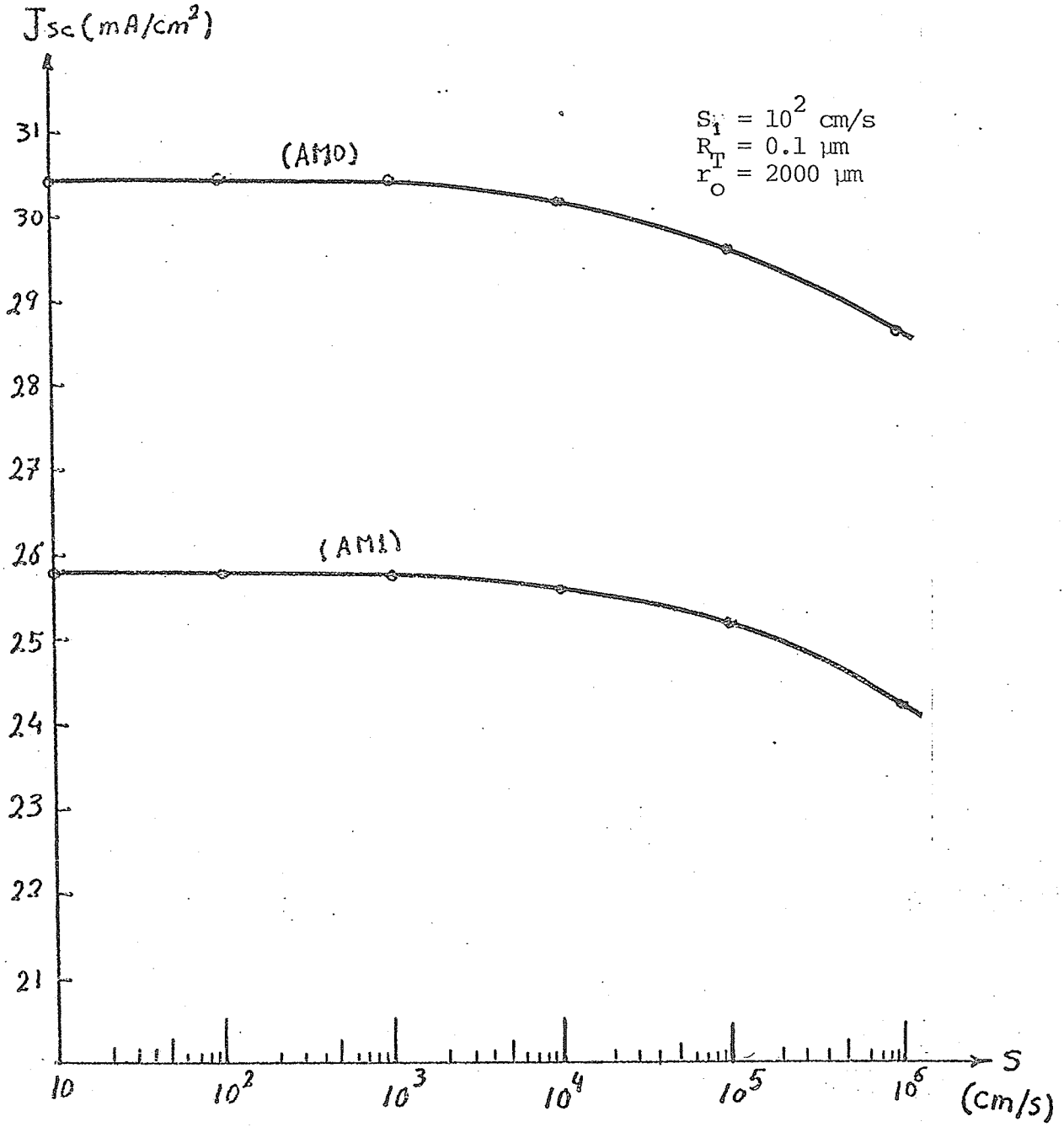

Fig. 21 Short circuit current as a function of surface recombination velocity S.

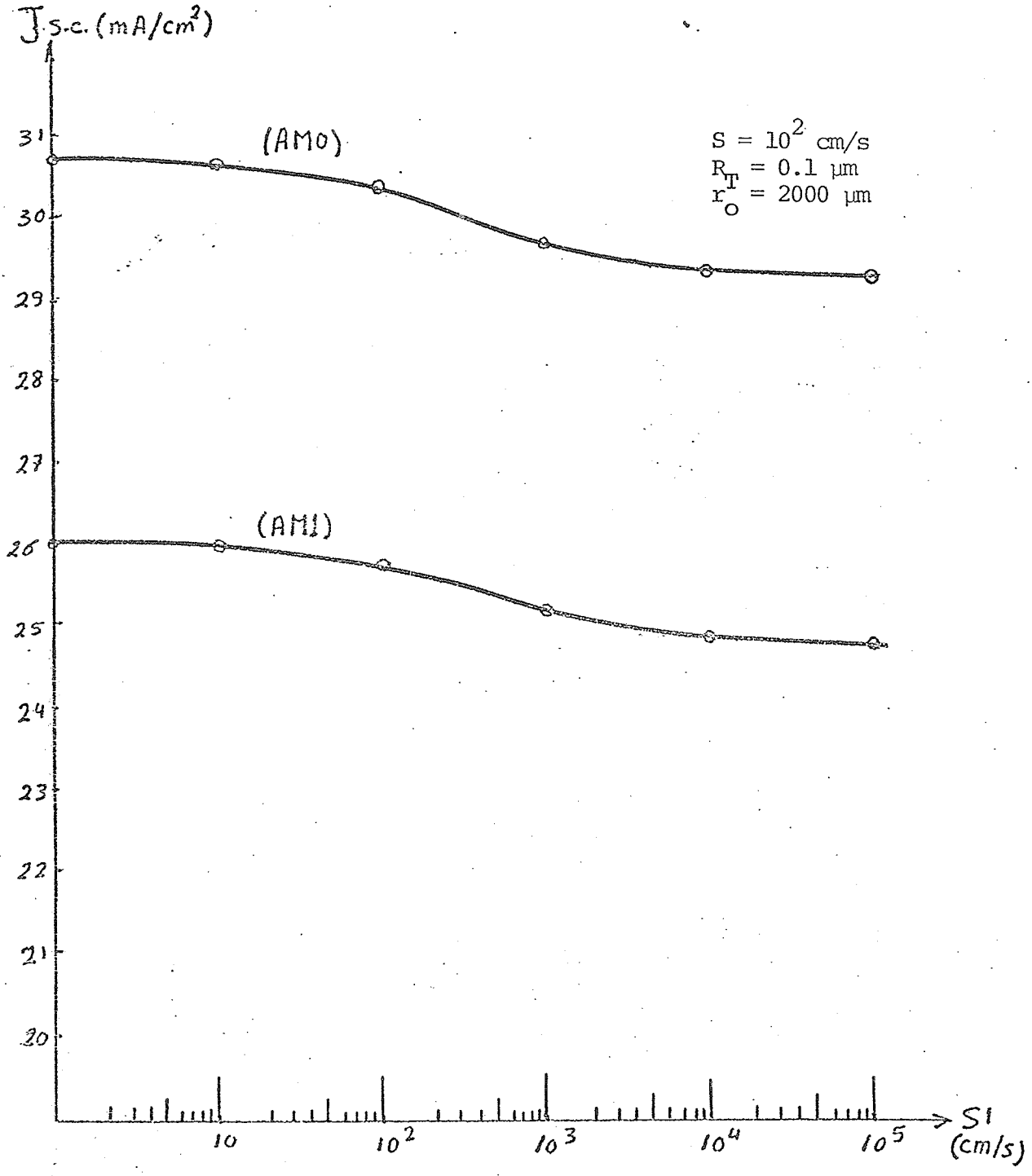

Fig. 22 Short circuit current as a function of surface recombination velocity Sl.

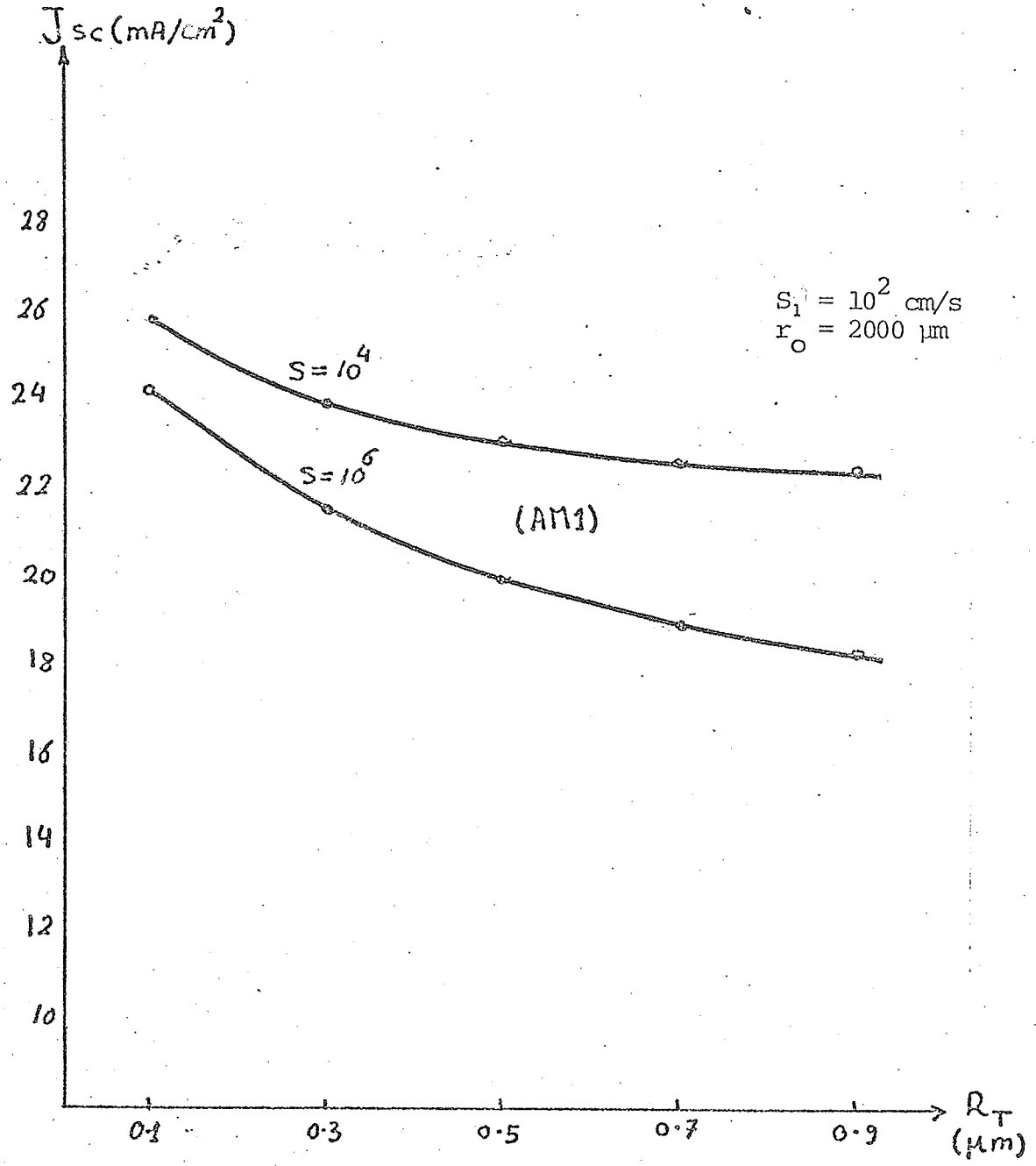

Fig. 23 Short circuit current as a function top thickness.

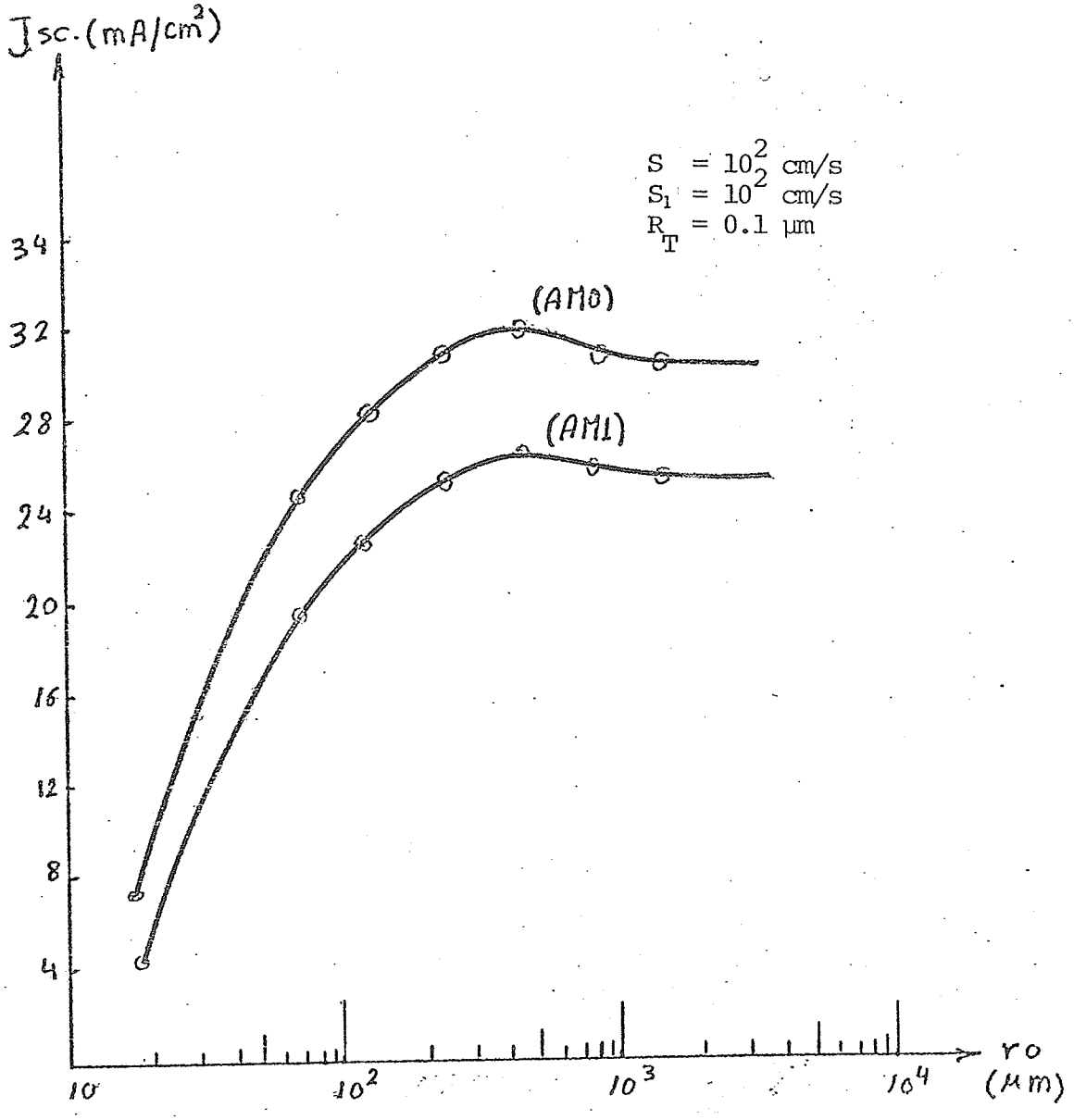

Fig. 24 Short circuit current as a function of cell radius.

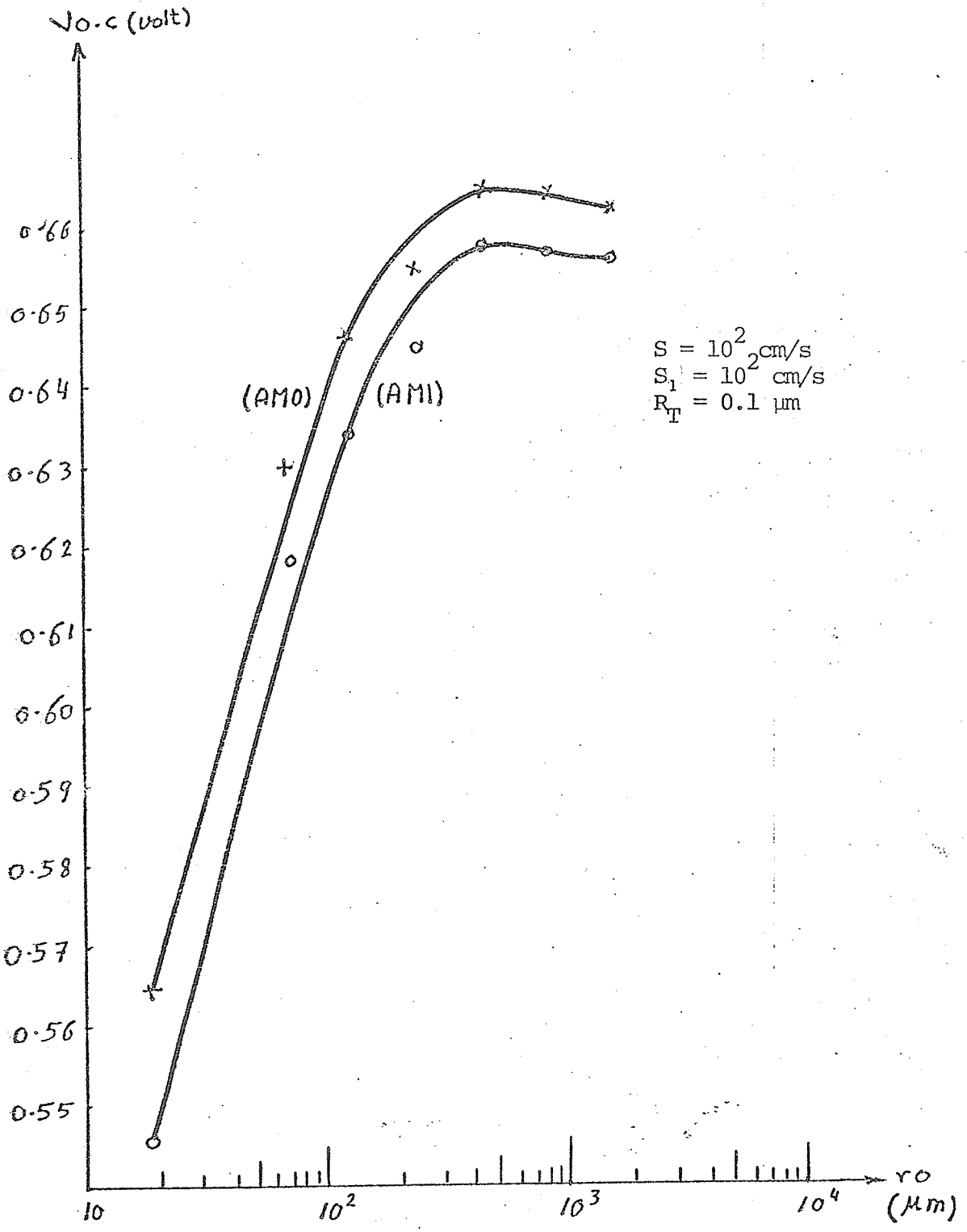

Fig. 25 Open circuit voltage as a function of cell radius.

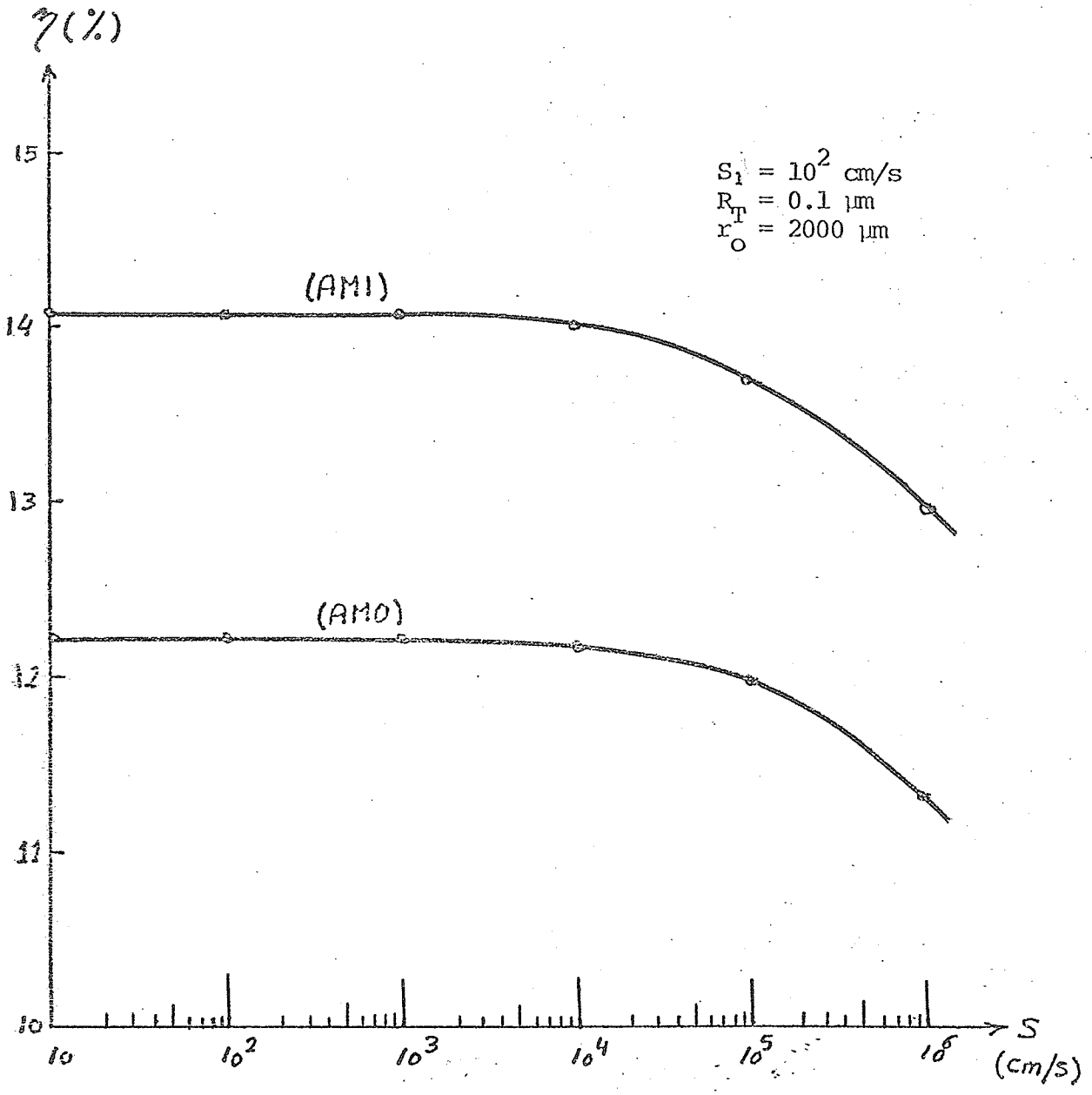

Fig. 26 Efficiency as a function of surface recombination velocity S.

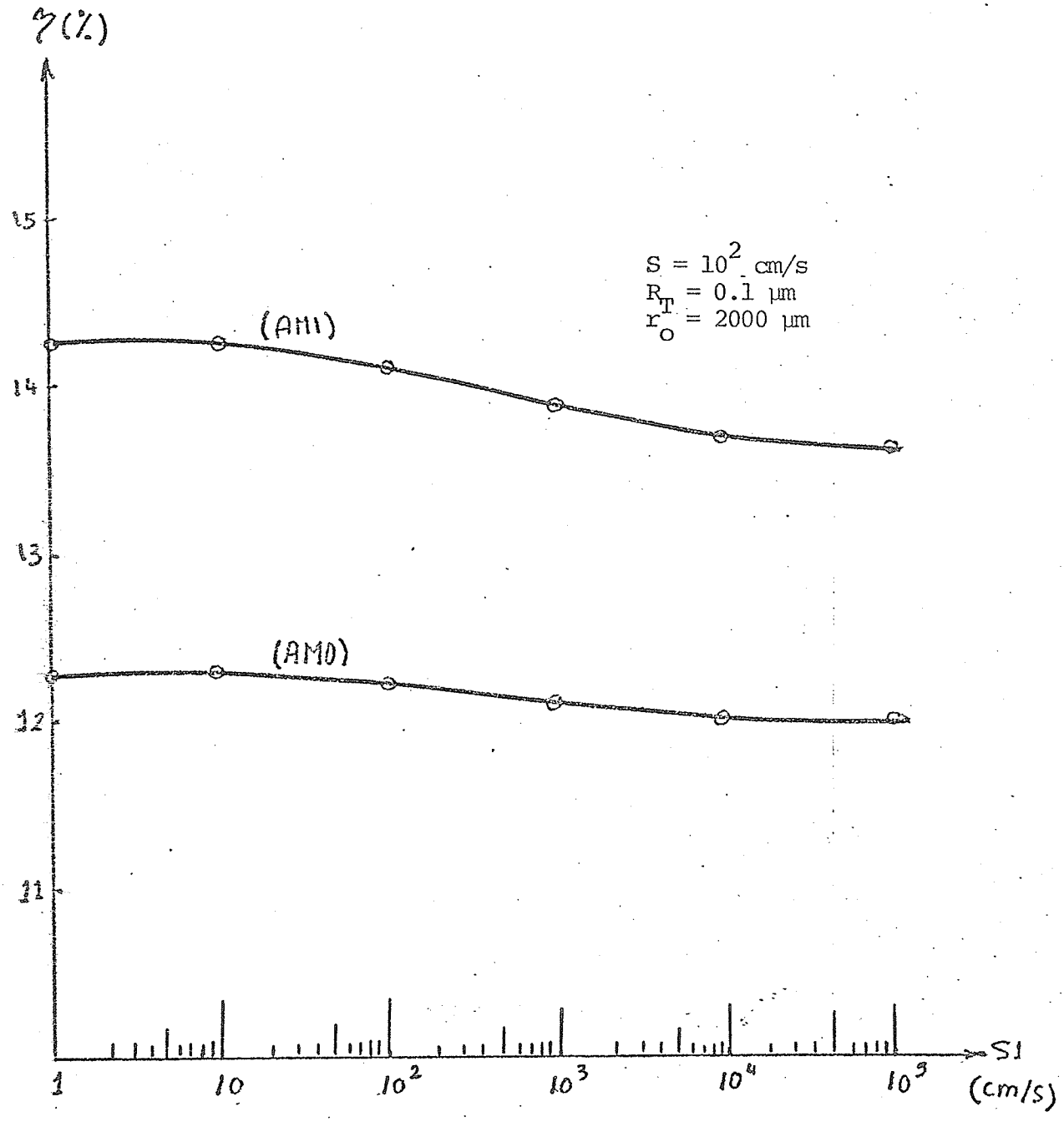

Fig. 27 Efficiency as a function of surface recombination velocity S1.

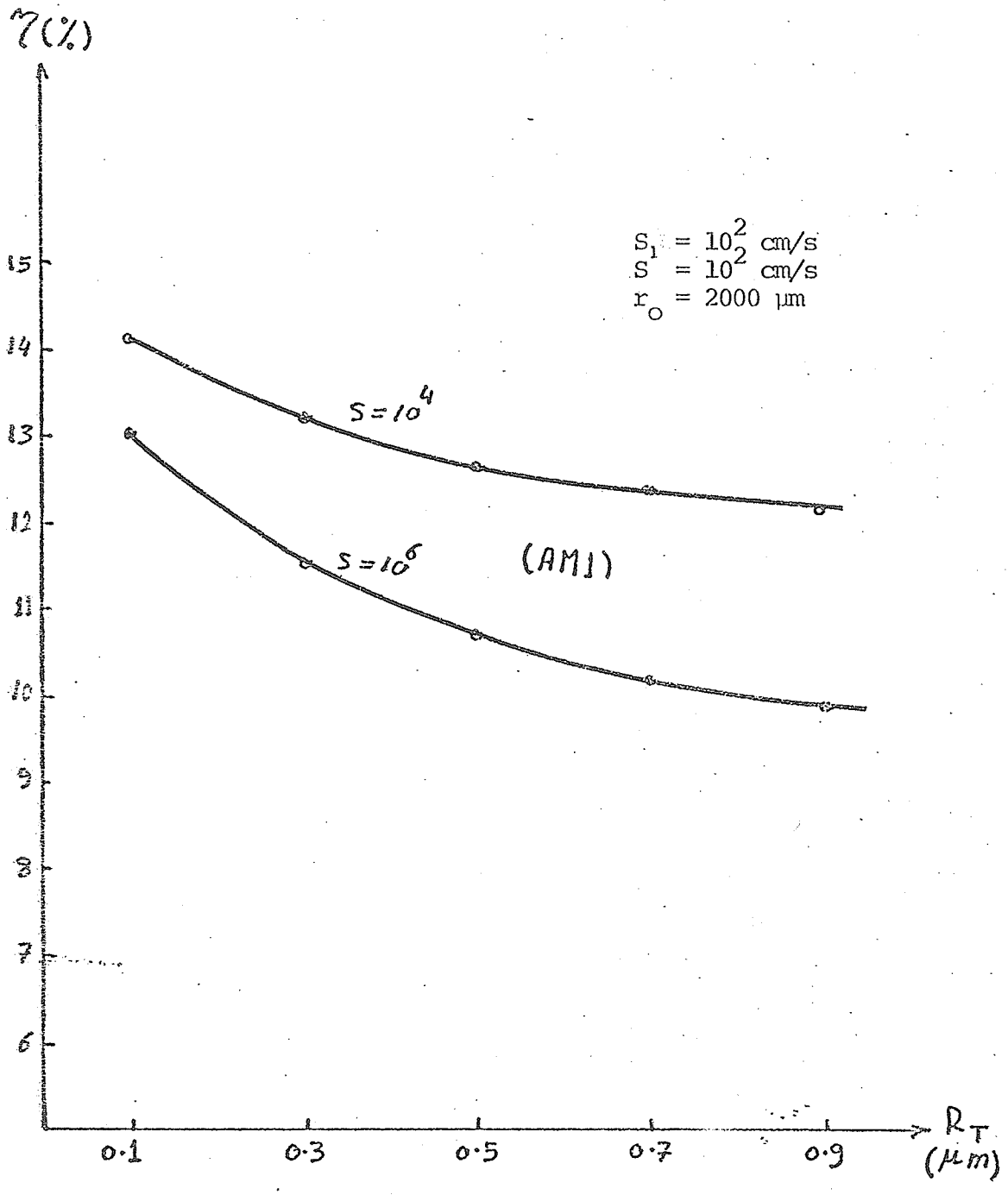

Fig. 28 Efficiency as a function of top region thickness.

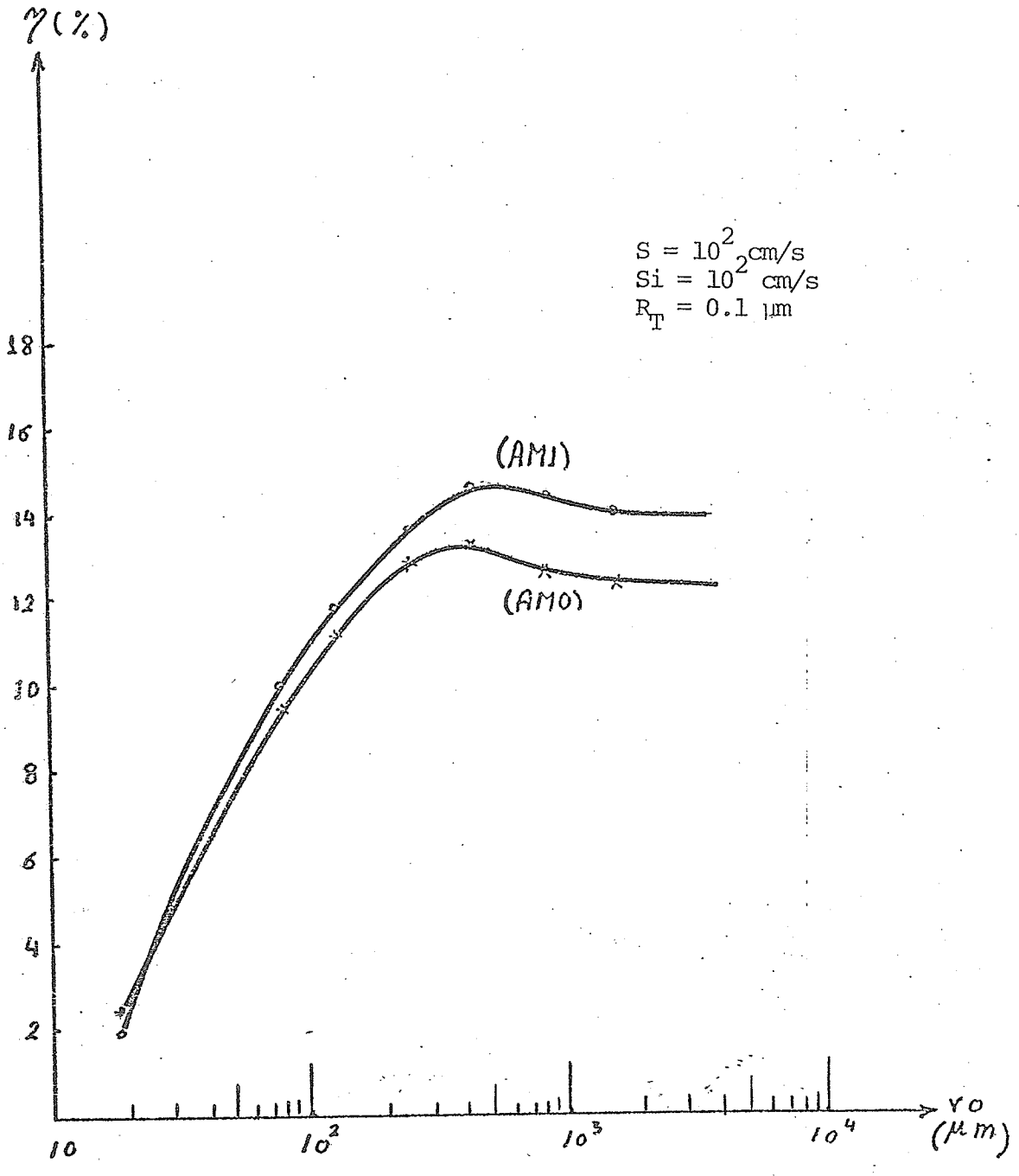

Fig. 29 Efficiency as a function of cell radius.

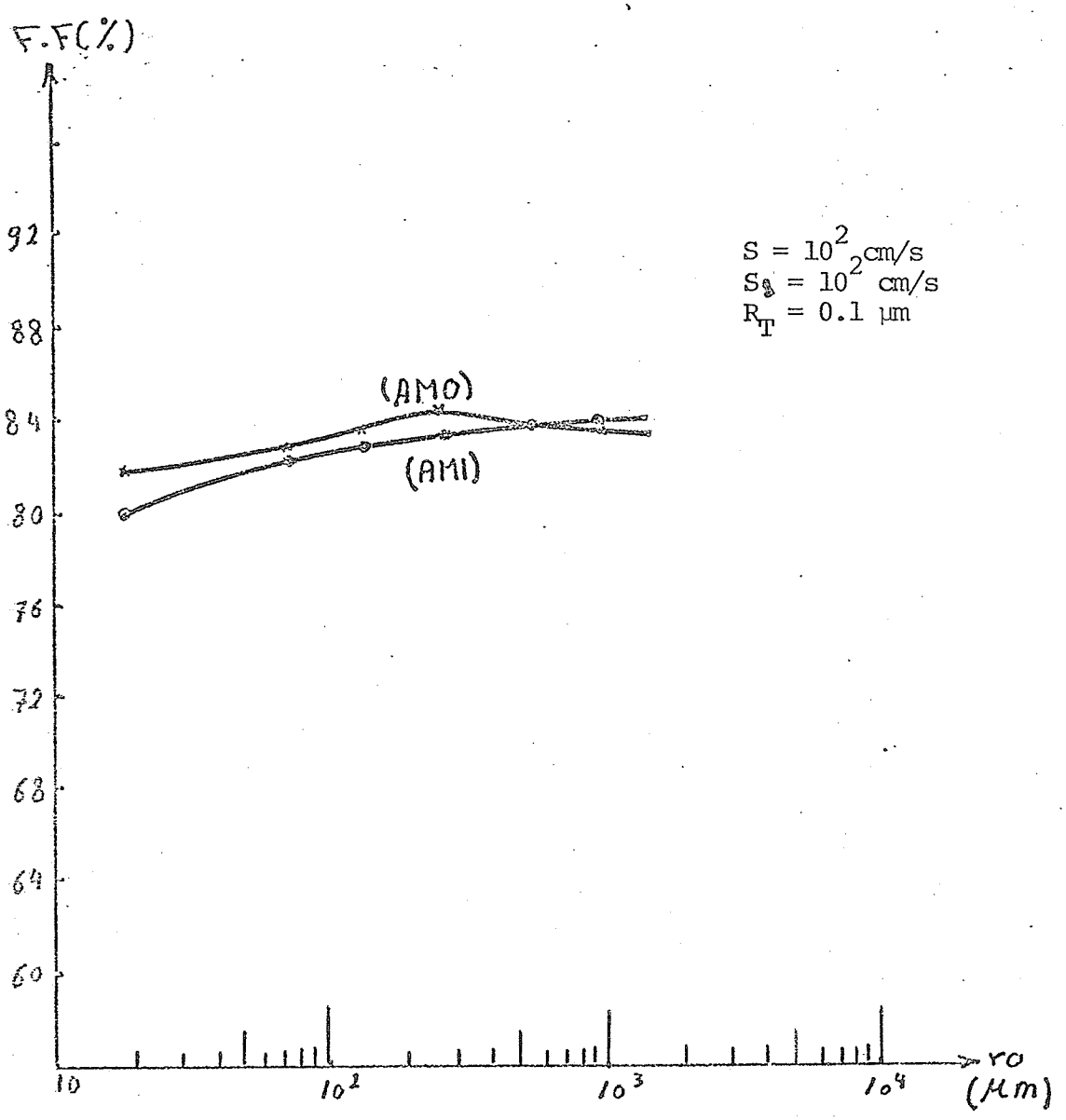

Fig. 30 Fill-Factor as a function of cell radius.

CONCLUSION AND SUGGESTION FOR FURTHER RESEARCH

From the previous results it is clear that the decrease of the surface recombination velocities S and S_1 lead to high values of efficiency and short circuit current, S and S_1 should therefore be as small as possible. This could be achieved by etching the surface. Also we should reduce the top thickness to obtain high I_{sc} and efficiency. The effect of radius is of great importance, giving us a maximum output power if the radius is around 500 μm. The dominant disadvantage of this cell is the series resistance. The series resistance for the half rod solar cell can be determined from equn(56), $R_s = \rho/(\pi\ell)$.

To avoid this problem we can construct a central region with very high doping levels. This region will lead to a low series resistance and will give a back surface field leading to high short circuit current and high open circuit voltage and consequently to high efficiency. This highly doped central region cell could be used in high intensity solar cell systems needing low series resistance. We could also use another material of low cost like a polycrystaline material or of high efficiency like the Ga As but in any case it is advisable to use a highly doped central region to improve performance.

We could use an induced electric field in the top region and in the base or in both, but the problem of series resistance remains. For optimum conditions we can use an induced electric field in the top and a central region of high doping in the base plus a radius around 500 μm.

REFERENCES

[1] H. J. Hovel, Solar cells, Vol. 11 of semiconductors and semimetals, Beer and Willardson, eds., Academic Press, N.Y., 1975.

[2] N. A. Abdel-Messih, Master Thesis, Faculty of Engineering, Cairo University, 1980.

[3] H. J. Hovel, Joint Conf. Am. Section, ISES and SES Canada, Inc., Winnipeg, August, 1976.

[4] S. Franz, G. Kent, and R. L. Anderson, Electronic materials conference, AIME, Salt Lake City, June 1976.

[5] C. T. Sah, R. N. Noyce, and W. Shockley, Proc. IRE 45, 1228 (1957).

[6] S. C. Choo, Solid State Electron. 11, 1009 (1968).

[7] A. G. Milnes and D. L. Feucht, "Heterojunctions and Metal-Semiconductor Junctions", Academic Press, New York, 1972.

[8] A. P. Thomas and M. P. Theka Kara, Proc. Joint Conf. Am. Section, ISES and SES Canada, Inc., Winnipeg, August 1976.

[9] M. Wolf, J. Vac. Sci. Technol., 12, 984 (1975).

[10] J. J. Wyoscki and P. Rappaport, J. Appl. Phys. 31, 571 (1960).

[11] S. M. Sze, Physics of Semiconductor devices, John Wiley and Sons, N. Y. 1969.

[12] A. S. Grove, "Physics and Technology of Semiconductor Devices", John Wiley, N.Y. 1967.

[13] H. Hinterberger and R. Winston, Rev. Sci. Inst. 37, 1094 (1966).

[14] V. K. Baranov and G. K. Mel'nikov, Sov. J. Opt. Tech. 33, 5 (1966).

[15] G. R. Johnson, M. G. Miles, D. P. Tanner, Photovoltaic Solar Energy Conference, page 259, Luxemburg, 1977.

[16] A. Gorski, R. Graven, W. McIntire, W. W. Schertz, R. Winston, and S. Zerdling, 12th IEEE Photovoltaic Specialists Conf., IEEE Cat. No. 76 CH 1142-7 ed., p. 764, 1977.

[17] Brice Carnahan, H. A. Luther, and James O. Wilkes, Applied Numerical Methods, John Wiley and Sons, Inc., N.Y. 1969.

APPENDIX (A)

DERIVATION OF EQUATION (45)

The number of photons absorbed by a hollow cylinder of unit length and dr thickness (Fig. (A.1)), can be written as

$$dN = 2\pi r I \alpha dr \tag{A.1}$$

where I is the photon intensity and r is the radius of the cylinder. This is equal to the differential of the number of incident photons at radius r which is

$$\begin{aligned} dN &= d(2\pi r I) \\ &= 2\pi r dI + 2\pi I dr \end{aligned} \tag{A.2}$$

equating (A.1) and (A.2) and dividing by the common factor, the result is

$$r I \alpha dr = r dI + I dr \tag{A.3}$$

dividing by rdr, (A.3) takes the form

$$\alpha I = \frac{dI}{dr} + \frac{I}{r} \tag{A.4}$$

therefore

$$\frac{dI}{dr} = I(\alpha - \frac{1}{r}) \tag{A.5}$$

putting $I = \frac{I'}{r}$, the L.H.S. of (A.5) becomes

$$\frac{dI}{dr} = \frac{1}{r}\frac{dI'}{dr} - \frac{1}{r^2} I' \tag{A.6}$$

and the R.H.S. of (A.5) becomes

$$I(\alpha - \frac{1}{r}) = \frac{I'}{r}(\alpha - \frac{1}{r})$$

so, equation (A.5) becomes

$$\frac{1}{r}\frac{dI'}{dr} - \frac{I}{r^2} I' = -\frac{I'}{r^2} + \frac{I'\alpha}{r} \tag{A.8}$$

cancelling equal terms on both sides,

$$\frac{dI'}{dr} = I'\alpha \tag{A.9}$$

or

$$\frac{dI'}{I'} = \alpha dr \tag{A.10}$$

the solution of equation (A.10) is

$$I' = I'_o \, e^{\alpha r} \tag{A.11}$$

and using $I = I'/r$, (A.11) this leads to

$$I = \frac{I'_o}{r} \, e^{\alpha r} \tag{A.12}$$

To determine I'_o one can use the boundary condition

$$I = F(1-R) \text{ at } r = r_o \tag{A.13}$$

substituting we have

$$F(1-R) = \frac{I'_o}{r_o} \, e^{\alpha r_o} \tag{A.14}$$

hence

$$I'_o = r_o \, F(1-R) \, e^{-\alpha r_o} \tag{A.15}$$

from equation (A.12) and (A.15), the intensity I at a radius r becomes

$$I = \frac{r_o}{r} \, F(1-R) \, e^{-\alpha(r_o - r)} \tag{A.16}$$

Assuming that every photon absorbed creates an electron hole pair, the density of electron hole pairs generated per second will be

$$\frac{dI}{dr} = \frac{r_o}{r} F(1-R)\left(\alpha - \frac{1}{r}\right) e^{-\alpha(r_o-r)} \qquad (A.17)$$

this equals the photogeneration rate G, which is

$$G(\lambda) = \frac{r_o}{r} F(\lambda)[1-R(\lambda)][\alpha(\lambda) - \frac{1}{r}] e^{-\alpha(\lambda)[r_o-r)} \qquad (A.18)$$

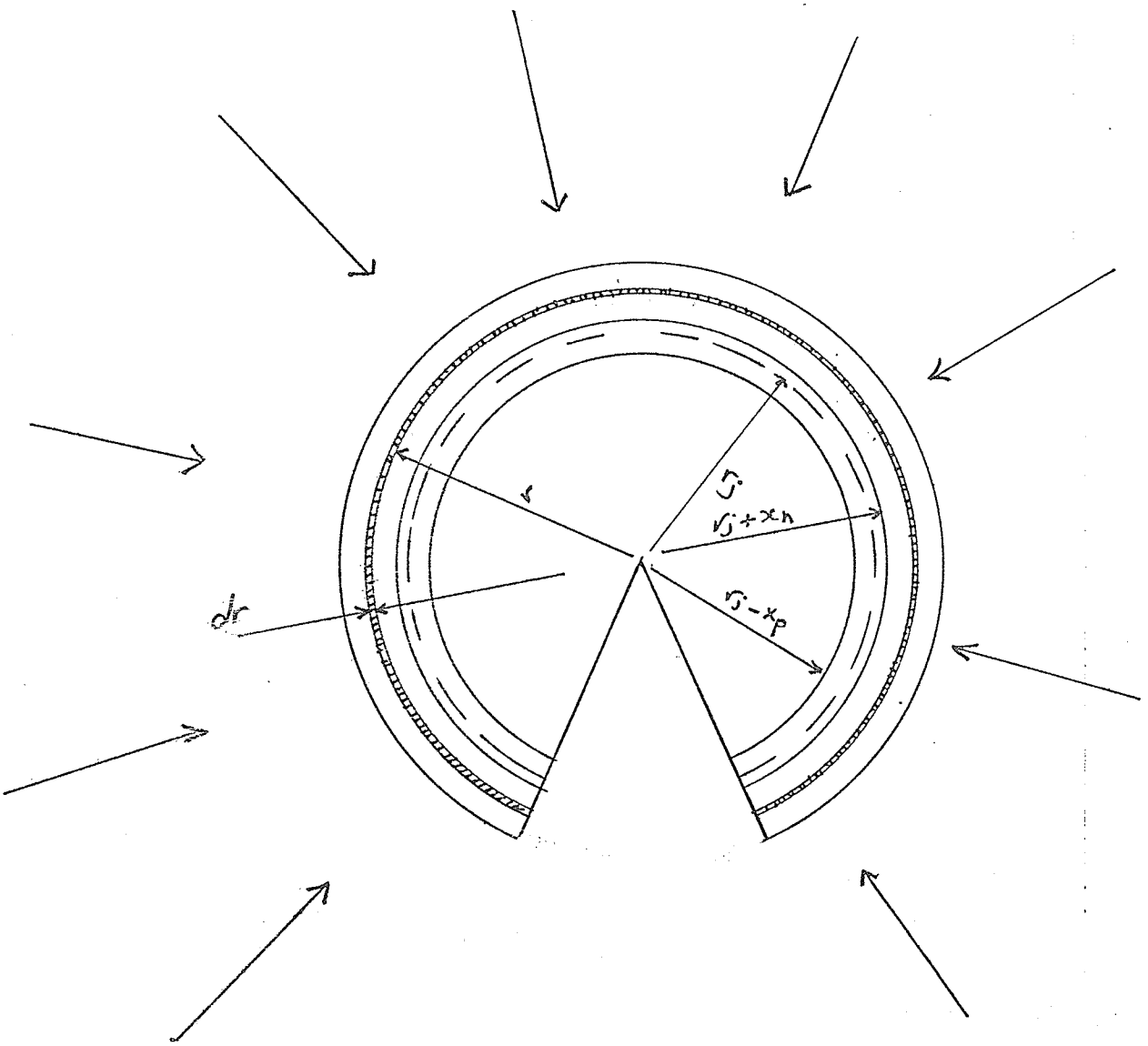

Fig. (A.1)

APPENDIX (B)

DERIVATION OF EQUATION (50)

Photon intensity at $r = r_j + x_n$ can be determined from equation (A.16) giving

$$I_1 = \frac{r_o}{r_j + x_n} F(1-R)\ e^{-\alpha(r_o - r_j - x_n)} \cdot \ell \qquad (B.1)$$

The total number of photon per second per unit length tall can be determined by multiplying equation (B.1) by $(r_j + x_n)\phi_{max}$ which gives

$$I_{1_{tot}} = \phi_{max}\ r_o\ F(1-R)\ e^{-\alpha(r_o - r_j - x_n)} \cdot \ell \qquad (B.2)$$

Similarly, the total number of photons per second per unit length at $r = r_j - x_p$ becomes

$$I_{2_{tot}} = \phi_{max}\ r_o\ F(1-R)\ e^{-\alpha(r_o - r_j + x_p)} \cdot \ell \qquad (B.3)$$

The number of photons absorbed by the depletion region is the difference between equations (B.2) and (B.3), which is equal to the number of electron hole pairs generated within the depletion region per second. If the electric field, inside the depletion region is high enough so that these pairs will not recombine, the difference between (B.2) and (B.3) will be equal to I_{rg}

therefore

$$I_{rg} = \phi_{max}\, r_o\, F(1-R)\, e^{-\alpha(r_o-r_j-x_n)} \cdot [1-e^{-\alpha w}] \cdot \ell \qquad (B.4)$$

APPENDIX (C)

THE NUMERICAL METHOD USED IN THE CALCULATION

(GAUSS-SEIDEL METHOD)

Dividing the r-ϕ plane of both the top and the base regions by M_1 & L_1 curves of constant r and by M_2 and L_1 lines of constant ϕ respectively as shown in Fig. (C.1), the derivatives of the excess minority carrier P and N w.r.t. r and ϕ can be expressed using Taylor's expansion. Expanding in Taylor's series for P(I-1, J) and P(I+1, J) about the central value, we obtain

$$P(I-1, J) = P(I, J) - \Delta r \frac{dP}{dr} + \frac{(\Delta r)^2}{2!} \frac{d^2P}{dr^2} - \frac{(\Delta r)^3}{3!} \frac{d^3P}{dr^3} + - - - \qquad (C.1)$$

neglecting the 3rd term in equation (C.1), the 1st derivative of P(I, J) w.r.t. r will be

$$\frac{dP}{dr} = \frac{P(I, J) - P(I-1, J)}{\Delta r} \qquad (C.2)$$

neglecting the 4th term in equation (C.1), and using equation (C.2), the 2nd derivative will be

$$\frac{d^2P}{dr^2} = \frac{P(I-1, J) - 2\,P(I, J) + P(I+1, J)}{(\Delta r)^2} \qquad (C.3)$$

Similarly the 2nd derivative w.r.t. ϕ becomes

$$\frac{d^2P}{d\phi^2} = \frac{P(I, J-1) - 2P(I, J) + P(I, J+1)}{(\Delta\phi)^2} \qquad (C.4)$$

Substituting equations (C.2), (C.3) and (C.4) in equation (43) we obtain

$$P(I, J)\left[\frac{-2}{(\Delta r)^2} - \frac{1}{r(\Delta r)} - \frac{2}{(r\Delta\phi)^2} - \frac{1}{D_p\tau_p}\right]$$

$$+ P(I+1, J)\left[\frac{1}{(\Delta r)^2} + \frac{1}{r\Delta r}\right] + P(I, J+1)\left[\frac{1}{(r\Delta\phi)^2}\right]$$

$$+ P(I, J-1)\left[\frac{1}{(r\Delta\phi)^2}\right] + P(I-1, J)\left[\frac{1}{(\Delta r)^2}\right]$$

$$+ \frac{G(I, J)}{D_p} = 0 \qquad (C.5)$$

Thus :

$$B = \frac{2}{(\Delta r)^2} + \frac{1}{r(\Delta r)} + \frac{2}{(r(\Delta\phi))^2} + \frac{1}{D_p\tau_p} \qquad (C.6)$$

$$B_1 = \frac{1}{(\Delta r)^2} + \frac{1}{r(\Delta r)} \qquad (C.7)$$

$$B_2 = \frac{1}{(\Delta r)^2} \qquad (C.8)$$

$$B_3 \quad \frac{1}{[r(\Delta\phi)]^2} \qquad (C.9)$$

$$C = \frac{G(I, J)}{D_p} \qquad (C.10)$$

$$A_1 = B_1/B \tag{C.11}$$

$$A_2 = B_2/B \tag{C.12}$$

$$A_3 = B_3/B \tag{C.13}$$

$$D = C/B \tag{C.14}$$

therefore equation (C.5) becomes

$$P(I, J) = A_1 \cdot P(I+1, J) + A_2 \cdot P(I-1, J)$$

$$+ A_3 \cdot P(I, J+1) + A_3 \cdot P(I, J-1) + D \tag{C.15}$$

Similarly equation (46.a) will be,

$$P(1, J) = \frac{1}{1 + s(\Delta r/D_p)} \; P(2, J) \tag{C.16}$$

equation (46.b) becomes,

$$P(M1, J) = 0 \tag{C.17}$$

equation (46.c) becomes,

$$P(I, 1) = 1/(1 + S_1 \frac{(\Delta\phi)r}{D_p}) \tag{C.18}$$

and equation (46.d) becomes

$$P(I, M_2) = 1/(1 + S_1 \frac{(\Delta\phi)r}{D_p}) \qquad (C.19)$$

by the same method it is easy to derive similar formulas for base region photocurrent and the dark currents for the two regions.

The method of solution is to iterate through all grid points, calculating a better approximation for the excess doping at each point (I, J) in turn from equation (C.15). As soon as a new value of P is calculated at a point, its previous value is discarded.

To start, a doping concentration of 0 is assumed everywhere within the boundary. The process of iteration through all grid points is repeated until further iteration hopefully change in the computed doping level. The calculation stops if every absolute value of all the grid points falls below a small quantity from its previously computed value. From these minority carrier concentration values we can calculate the current for a specific wavelength. Total current can be calculated by summing over all the wavelengths. In the same way we can calculate the dark current for certain applied voltages.

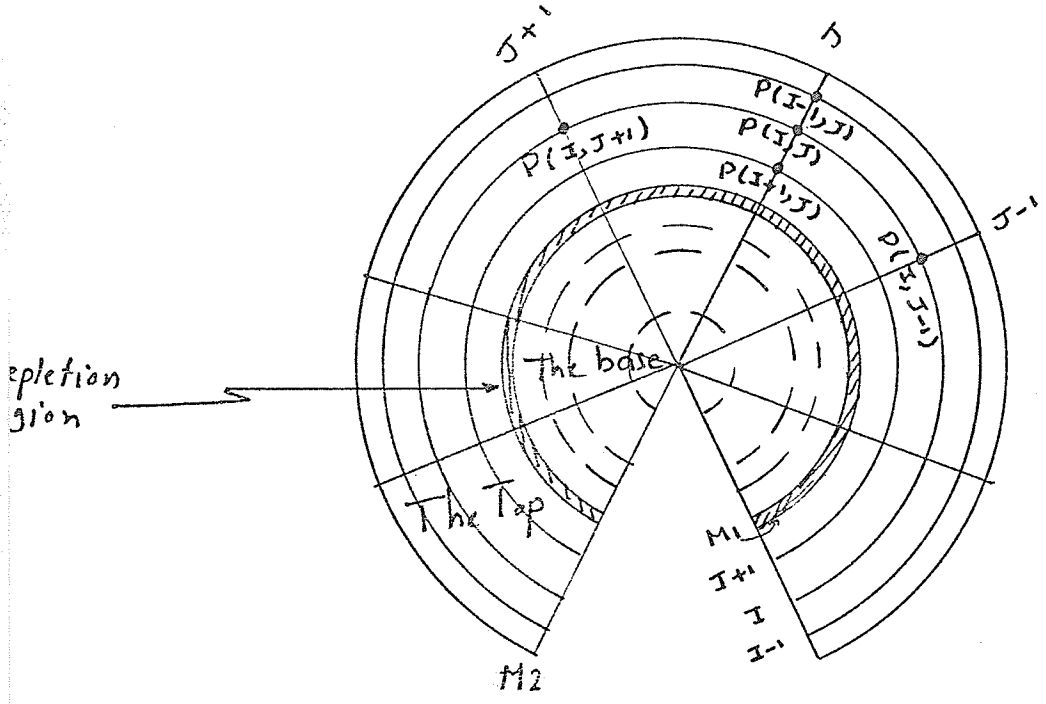
J+1
J
J-1
P(I-1,J)
P(I,J+1)
P(I,J)
P(I+1,J)
P(I,J-1)
epletion
gion
The base
The Top
M1
M2
I+1
I
I-1

Fig. (C.1)